

# 國立交通大學

電信工程學系

碩士論文

槽孔耦合多頻帶手機天線

**A Coupling Slot Multiband Antenna for Mobile Phones**

研究生：詹兆凱

指導教授：唐震寰 教授

中華民國九十八年七月

槽孔耦合多頻帶手機天線

A Coupling Slot Multiband Antenna for Mobile Phones

研究生：詹兆凱

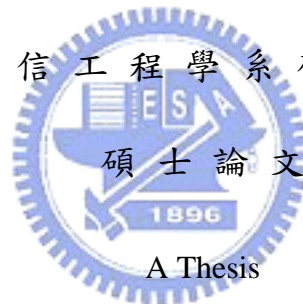
Student : Chao-Kai Chan

指導教授：唐震寰 博士

Advisor : Dr. Jenn-Hwan Tarn

國立交通大學

電信工程學系碩士班



Submitted to Department of Communication Engineering  
College of Electrical Engineering and Computer Science  
National Chiao Tung University  
in Partial Fulfillment of the Requirements  
for the Degree of  
Master  
in

Communication Engineering

July 2009

Hsinchu, Taiwan, Republic of China

中華民國九十八年七月

# 槽孔耦合多頻帶手機天線

研究生：詹兆凱

指導教授：唐震寰 教授

國立交通大學

電信工程學系 碩士班

## 摘要

本論文提出一個應用於手機的槽孔天線設計。天線為在接地面上挖兩個L形的槽孔及一個寄生元件所組成。經由適當的設計，兩個L形的槽孔可由耦合效應激發所需的操作頻帶。另外，寄生元件可由接地面上的槽孔經電磁耦合效應下，激發出WLAN頻帶。因此，三個輻射元件可以各別激發出三個共振模態，中心頻率分別為 900MHz，2100MHz，5200MHz，涵蓋的頻段為 GSM/DCS/PCS/UMTS/Bluetooth/WiMAX/WLAN。而天線為簡單的平面架構，所占面積為 $35\times 22\text{mm}^2$ ，且所操作的三個頻帶的輻射特性良好。本天線的設計細節及實驗結果在論文中詳細討論。

# **A Coupling Slot Multiband Antenna for Mobile Phones**

Student: Chao-Kai Chan

Advisor: Dr. Jenn-Hwan Tarn

Department of Communication Engineering

National Chiao Tung University

## **Abstract**

A novel internal multiband slot antenna for mobile phone applications is presented. The antenna consists of two L-shaped slots of different lengths cut at the edge of the system ground and added a parasitic strip. It is shown that with a proper design, the two L-shaped slots can generate the operating bandwidths by coupling effect. And the parasitic strip is electromagnetically coupled and excited by the slot to generate the WLAN band. Hence, three elements can separately control the operating frequencies of the three excited resonant modes, which generate the three bands centered at about 900, 2100 and 5200 MHz to cover the GSM/DCS/PCS/UMTS/Bluetooth/WiMAX/WLAN bands. Furthermore, the antenna has a simple planar structure and occupies a small area of  $35 \times 22 \text{mm}^2$ . Good radiation characteristics are obtained over the three operating bands. The design details for the proposed antenna are described, and the experimental results of the antenna performances are presented and discussed.

## 誌 謝

在碩士班研究的這二年歲月，首先要感謝的是我的指導教授 唐震寰教授並致上我最誠摯的謝意。感謝老師在專業的通訊領域中，給予我不斷的指導與鼓勵，並賦予了實驗室豐富的研究資源與環境，使得這篇碩士論文能夠順利完成。同時，亦感謝口試委員國立臺灣大學 李學智教授及國立臺灣科技大學 楊成發教授對於論文內容所提出的寶貴建議及指導，在此致上最誠懇的謝意。

其次，要感謝實驗室的學長們——佩宗學長、清標學長、育正學長、志瑋學長、豐吉學長、奕慶學長、雅仲學長、俊諺學長、威聰學長、智偉學長、稟文學長、文崇學長、瑞榮學長、松融學長等在研究上的幫助與意見，讓我獲益良多。感謝實驗室的同學——振銘、明宗、廣琪等在課業及研究上的互相砥礪與切磋，以及生活上的多彩多姿，另外要感謝炳志在量測天線時的幫忙。亦感謝學弟們——耿賢、鈺泓、冠豪、國政，讓實驗室在嚴肅的研究氣氛中增添了許多歡樂，有了你們，更加豐富了我這二年的研究生生活。另外，也要感謝助理——梁麗君小姐，在實驗室上的協助和籌劃每次的美食聚餐饗宴。

最後，要感謝的就是我最親愛的家人。他們在我求學過程中，一路陪伴著我，給予我最溫馨的關懷與鼓勵，讓我在人生的過程裡得到快樂，更讓我可以專心於研究工作中而毫無後顧之憂。

鑒此，謹以此篇論文獻給所有關心我的每一個人。

詹兆凱 誌予

九十八年七月

# CONTENTS

ABSTRACT (CHINESE).....	I
ABSTRACT (ENGLISH).....	II
ACKNOWLEDGEMENT.....	III
CONTENTS.....	IV
LIST OF TABLES.....	V
LIST OF FIGURES.....	VI



<b>CHAPTER 1 Introduction</b>	<b>1</b>
1.1 Background and Problems.....	1
1.2 Related Works.....	2
1.3 Thesis Organization.....	3
<b>CHAPTER 2 Basics of Slot Antennas</b>	<b>4</b>
2.1 Introduction.....	4
2.1.1 Radiation fields of slot antennas.....	4
2.1.2 The impedance of slot antennas.....	6
2.1.3 Patterns of Slot antennas.....	9

2.1.4 Microstrip-to-slot Cross-Junction Transition.....	10
2.2 High-Performance Techniques.....	13
<b>CHAPTER 3 Review of Multi-band Antenna for Mobile Phones</b>	<b>21</b>
<hr/>	
3.1 Literature Review.....	21
<b>CHAPTER 4 The Proposed Slot Antenna</b>	<b>29</b>
<hr/>	
4.1 Antenna Configuration and operation.....	29
4.2 Design Considerations and Procedure.....	32
4.3 Experimental Results and Discussions.....	35
4.4 Summary.....	44
<b>CHAPTER 5 Conclusion</b>	<b>45</b>
<hr/>	
<b>REFERENCES.....</b>	<b>46</b>

## List of Tables

Table 3.I Comparison of various multiband antennas.....	28
Table 4.I Design Parameters.....	30
Table 4.II Peak Gain.....	40
Table 4.III Comparison I.....	44
Table 4.IV Comparison II.....	44

## List of Figures

Figure 2.1	Center-fed-slot.....	5
Figure 2.2	Slot antenna and complementary dipole antenna.....	6
Figure 2.3	Radiation fields of a (a) $\lambda/2$ slot on a screen and (b) a $\lambda/2$ flat dipole.....	9
Figure 2.4	Microstrip-to-slot transition.....	10
Figure 2.5	Transmission line equivalent circuit for the transition of Fig. 2.4.....	11
Figure 2.6	Reduced equivalent circuit of Fig. 2.5.....	11
Figure 2.7	Transformed equivalent circuit of Fig. 2.6.....	12
Figure 2.8	Transmission line model of a slot antenna (a) half-wave slot antenna. (b) Inductively terminated slot antenna. (c) Two series inductive terminations.....	14
Figure 2.9	The geometry of the antenna and its feed designed to operate at 300MHz.....	14
Figure 2.10	Electric field distributions and three-dimensional geometry of a microstrip-fed slot antenna (a) Normal field distribution (b) Field distribution at a slightly higher frequency showing a fictitious short circuit along the slot causing the second resonance (c) Three-dimensional geometry.....	15
Figure 2.11	Geometry of the straight, L and T shapes slot antennas.....	16
Figure 2.12	Geometry of the band-rejected open slot antenna for WLAN bands...17	17
Figure 2.13	Measured return loss for various lengths (L3) of the antenna.....	17
Figure 2.14	(a) Top view, (b) side view, (c) limped-element equivalent circuit model for the rectangular slot type radiator, and (d) total equivalent circuit of the rectangular slot type harmonic suppressed antenna.....	18



Figure 2.15	Simulated return losses for (a) L and (b) W of the rectangular slot type HAS.....	19
Figure 2.16	(a) Geometry of the multiband printed monopole slot antenna for WWAN (wireless wide area network) operation in the laptop computer (b) Dimensions of the antenna.....	20
Figure 2.17	Measured and simulated return loss for the proposed antenna.....	20
Figure 3.1	Geometry of the triple-band antenna (a) 3-D view, (b) fabricated internal monopole antenna, (c) unfolded structure of radiating elements.....	22
Figure 3.2	Surface current distributions on the radiating elements for triple-resonant antenna: (a) 930 MHz, (b) 1850 MHz, (c) 2630 MHz.....	23
Figure 3.3	Comparison between measured and simulated results of triple-resonant antenna.....	23
Figure 3.4	(a) Geometry of the proposed folded loop chip antenna (b) Detailed dimensions of the antenna unfolded into a planar structure.....	24
Figure 3.5	Measured and simulated return loss for the proposed antenna.....	25
Figure 3.6	Geometry of the antenna .....	25
Figure 3.7	Comparison between the measured and simulated return losses.....	26
Figure 3.8	(a) Geometry of the proposed printed monopole slot antenna for mobile phone application (b) Side view of the geometry in (a) with a 1-mm-thick plastic housing (c) Detailed dimensions of the antenna.....	27
Figure 3.9	Measured and simulated return loss for the antenna; the 1-mm-thick plastic housing is included.....	27
Figure 4.1	Geometry of the proposed printed slot antenna.....	30

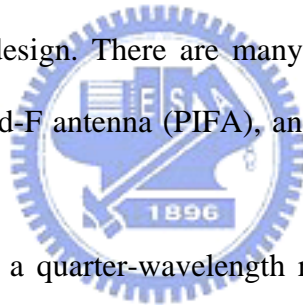
Figure 4.2	Photographs of the fabricated antenna (a) top view (b) back view.....	31
Figure 4.3	Surface current distribution at 900MHz.....	32
Figure 4.4	Surface current distribution at 2100MHz.....	33
Figure 4.5	Surface current distribution at 5200MHz.....	34
Figure 4.6	Surface current distribution of the parasitic strip at 5200MHz .....	34
Figure 4.7	Simulated and measured return loss for the proposed antenna .....	36
Figure 4.8	Geometry of the proposed slot antenna with a 1-mm-thick plastic housing .....	37
Figure 4.9	Simulated return loss of the proposed antenna w/o plastic housing ...	37
Figure 4.10	A conducting box (PEC) of size $33 \times 30 \times 6 \text{ mm}^3$ on the ground is used to simulate the battery case .....	38
Figure 4.11	Simulated return loss of the proposed antenna with and without a conducting box of size $33 \times 30 \times 6 \text{ mm}^3$ placed on the ground as a battery.....	39
Figure 4.12	Simulated and measured radiation patterns .....	43

## Chapter 1 Introduction

---

### 1.1 Background and Problems

Modern mobile phones have developed rapidly during the past decade. The demand of compact, light weight, reduced height, and multifunctional phones puts more stringent requirements on the antenna design. There are many kinds of multiband antennas such as monopole, loop, planar inverted-F antenna (PIFA), and slot antennas, which we will discuss below.



The monopole antenna is a quarter-wavelength resonant mode, which is based on the image theory. It is straightforward to achieve multiband by generating multipath for operating bands. But it is difficult to independently control the different resonant frequencies because of the mutual coupling between the radiators of the antenna. The loop antenna can be configured to be a chip antenna, which is a one-wavelength resonant mode for mobile phone applications. However, it comprises a folded loop strip attached on a foam base, which is difficult to fabricate.

Being compact and low profile, planar inverted-F antenna (PIFA) is a potential structure as a basic element to realize multiband personal communication handset antennas. However, the conventional PIFA structure has a shorting pin to feed ground, which makes the antenna as a three dimensional structure. The height of shorting pin not only affects the impedance bandwidth but also increases the antenna volume. Additionally, we need a via-hole to connect

the shorting pin, which makes fabrication more difficult.

It has been known that the slot antenna is traditionally operated at its half-wavelength fundamental resonant mode. Recent years have seen increased attention being given to the slot antenna for mobile phone applications. It is shown that the slot antenna with its one end open-ended can generate a quarter-wavelength resonant mode. In addition, the microstrip-line-fed slot antennas possess advantages such as wide impedance bandwidth, low profile, light weight, low cost, and ease of fabrication. This feature is advantageous over the conventional internal antennas; for example, the planar inverted-F antennas (PIFAs) have been applied in many mobile phones. The compact size and simple planar structure make it promising for application in the mobile devices. In view of the above discussions, we select the slot antenna as our approach to multiband antenna. In this thesis, we present a promising design of the slot antenna for multiband operation in the mobile phone.

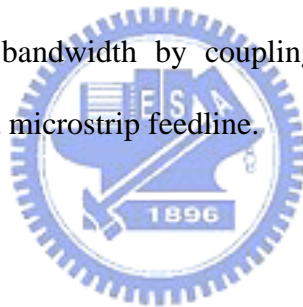


## **1.2 Related Works**

In recent years, an increasing number of recent publications and studies have reassessed the positive contribution that slot antennas can make to mobile applications. The reason is that the slot antenna has a simple planar structure and is suitable to be printed on the system circuit board of the mobile device, which makes it easy to fabricate at low cost for practical applications.

The papers [2], [3] in Wong (2007, 2009) provide extensive discussions of the applications of slot antennas. In [2], the antenna consists of two slots cut at the edge of the ground plane of different lengths and is printed on the system circuit board. A quarter-wavelength slot antenna can be obtained by cutting the slot at the edge of the ground plane. A  $50\Omega$  microstrip feedline printed at the location away from the edge of the ground

plane is used to excite the two slots. The longer and shorter slot controls the excitation of the lower band and upper band, respectively. It is true that the proposed antenna's structure [2] is compact and simple. However, the impedance bandwidth may be degraded due to the additional WLAN band by cutting another slot on the ground. In order to alleviate the degradation due to the mutual coupling between slots on the same layer, we employ the parasitic strip to generate WLAN band without degrading other impedance bandwidth. In [3], it demonstrates that the slot antenna is also promising for application in the laptop computer as an internal antenna for WWAN (wireless wide area network) operation. The operation is similar to [2], but the step-shaped microstrip feedline is applied to excite the three slots at their respective optimal feeding position. Instead of utilizing the step-shaped microstrip feedline [3] to excite the slots at their optimal feeding position, we use a short L-shaped slot to excite a wide impedance bandwidth by coupling. It is easier to tune the operating bandwidth than the step-shaped microstrip feedline.



### **1.3 Organization of Thesis**

The thesis is organized as follows. In Chapter 2, we describe basic physics and introduce improved techniques for slot antennas. And then we review a variety of types for multiband antennas in Chapter 3. In Chapter 4, we present the design of the proposed antenna and the experimental results. Finally, Chapter 5 concludes this study and draws some possible future works.

## Chapter 2 Basics of Slot Antennas

---

### 2.1 Introduction

In this section, we deal with the basic physics and operation of a slot antenna such as radiation fields, impedance, patterns of slot antennas, and microstrip-to-slot transition [4]-[7].

#### 2.1.1 Radiation fields of slot antennas

Let us consider the radiation from a center-fed slot in the ground plane (Fig. 2.1). The electric field in the slot is given by

$$E_x = \frac{V_0}{w} \frac{\sin k(l-|z|)}{\sin kl}. \quad (2.1)$$

This is identical to the magnetic current  $J_m$  in front of the ground plane.

$$J_m = \bar{E} \times \hat{n} = E_x \hat{x} \times \hat{y} = E_x \hat{z} \quad (2.2)$$

This is equivalent to the magnetic current  $J_m$  and its image in free space. Hence, the field is equal to the field generated by  $2J_m$ . Utilizing (2.3) for radiation field  $E_\theta$  and  $E_\phi$  due to

$$\vec{J}(\vec{r}') \text{ and } \vec{J}_m(\vec{r}')$$

$$\begin{aligned}
 E_{\theta} &= -\frac{j\omega\mu_0}{4\pi R} e^{-jkR} \int \hat{\theta} \cdot \vec{J} \left( \vec{r}' \right) e^{jk\hat{r} \cdot \vec{r}'} dV' - \frac{jk}{4\pi R} e^{-jkR} \int \hat{\phi} \cdot \vec{J}_m \left( \vec{r}' \right) e^{jk\hat{r} \cdot \vec{r}'} dV' \\
 E_{\phi} &= -\frac{j\omega\mu_0}{4\pi R} e^{-jkR} \int \hat{\phi} \cdot \vec{J} \left( \vec{r}' \right) e^{jk\hat{r} \cdot \vec{r}'} dV' + \frac{jk}{4\pi R} e^{-jkR} \int \hat{\theta} \cdot \vec{J}_m \left( \vec{r}' \right) e^{jk\hat{r} \cdot \vec{r}'} dV'
 \end{aligned}
 \tag{2.3}$$

We have

$$\begin{aligned}
 E_{\theta} &= 0 \\
 E_{\phi} &= -j \frac{e^{-jkR}}{\pi R} V_0 \frac{\cos(kl \cos \theta) - \cos kl}{\sin kl \sin \theta}
 \end{aligned}
 \tag{2.4}$$

The magnetic field  $\vec{H}$  in the far field is simply related to  $\vec{E}$ :

$$\vec{H} = \frac{1}{\eta} \hat{r} \times \vec{E}, \quad \eta = \sqrt{\frac{\mu_0}{\epsilon_0}}
 \tag{2.5}$$

Therefore,

$$\begin{aligned}
 H_{\theta} &= -\frac{E_{\phi}}{\eta} = j \frac{e^{-jkR}}{\eta \pi R} V_0 \frac{\cos(kl \cos \theta) - \cos kl}{\sin kl \sin \theta} \\
 H_{\phi} &= \frac{E_{\theta}}{\eta} = 0
 \end{aligned}
 \tag{2.6}$$

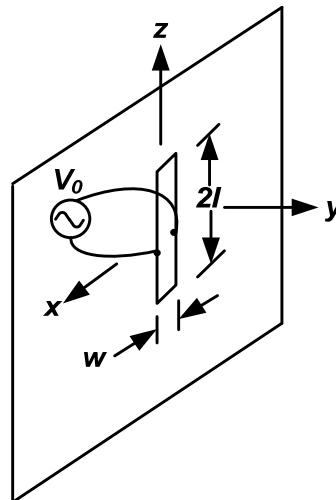


Fig. 2.1 Center-fed-slot

### 2.1.2 The impedance of slot antennas

Consider the slot antenna and the complementary dipole antenna shown in Fig. 2.2. The terminals of each antenna are indicated by  $FF$ , and it is assumed that they are separated by an infinitesimal distance. It is assumed that the dipole and slot are cut from an infinitesimally thin, plane, perfectly conducting sheet.

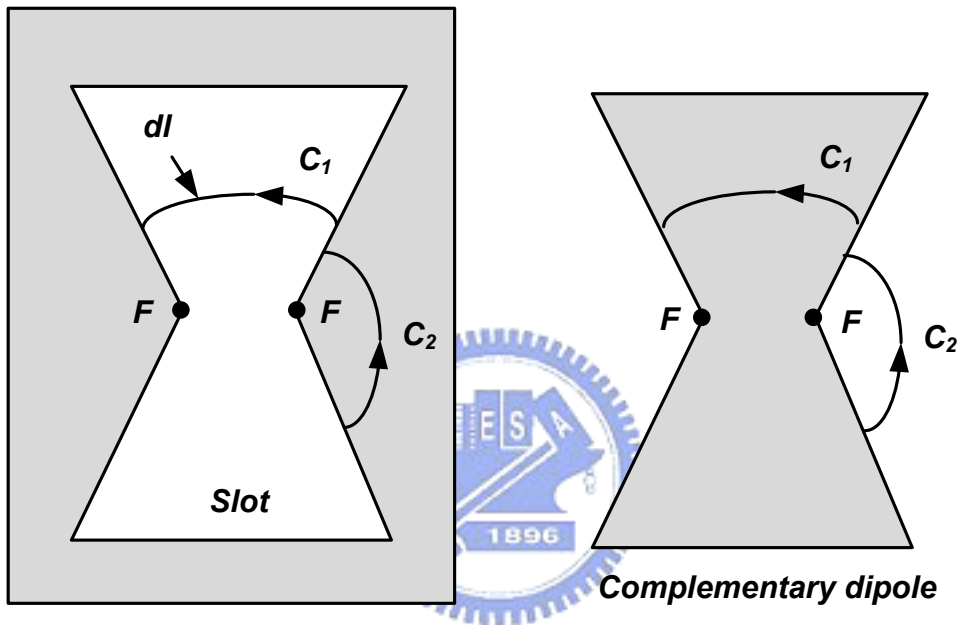


Fig. 2.2 Slot antenna and complementary dipole antenna

Let a generator be connected to the terminals of the slot. The driving-point impedance  $Z_s$  at the terminals is the ratio of the terminal voltage  $V_s$  to the terminal current  $I_s$ . Let  $\mathbf{E}_s$  and  $\mathbf{H}_s$  be the electric and magnetic fields of the slot at any point  $P$ . Then the voltage  $V_s$  at the terminals  $FF$  of the slots is given by the line integral of  $\mathbf{E}_s$  over the path  $C_1$  as  $C_1$  approaches zero. Thus,

$$V_s = \lim_{C_1 \rightarrow 0} \int_{C_1} \mathbf{E}_s \cdot d\mathbf{l} \quad (2.7)$$

where  $d\mathbf{l}$  = infinitesimal vector element of length  $d\mathbf{l}$  along the contour or path  $C_1$ .

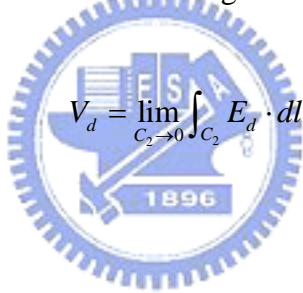


The current  $I_s$  at the terminals of the slot is

$$I_s = 2 \lim_{C_2 \rightarrow 0} \int_{C_2} H_s \cdot dl \quad (2.8)$$

The path  $C_2$  is outside the metal sheet and parallel to its surface. The factor 2 enters since only 1/2 of the closed line integral is taken, the line integral over the other side of the sheet being equal by symmetry.

Now consider the complementary dipole antenna. Let a generator be connected to the terminals of the dipole. The driving-point impedance  $Z_d$  at the terminals is the ratio of the terminal voltage  $V_d$  to the terminal current  $I_d$ . Let  $\mathbf{E}_d$  and  $\mathbf{H}_d$  be the electric and magnetic fields of the dipole at any point  $P$ . Then the voltage at the dipole terminals is



$$V_d = \lim_{C_2 \rightarrow 0} \int_{C_2} E_d \cdot dl \quad (2.9)$$

, and the current is

$$I_d = 2 \lim_{C_1 \rightarrow 0} \int_{C_1} H_d \cdot dl \quad (2.10)$$

However,

$$\lim_{C_2 \rightarrow 0} \int_{C_2} E_d \cdot dl = Z_0 \lim_{C_2 \rightarrow 0} \int_{C_2} H_s \cdot dl \quad (2.11)$$

And

$$\lim_{C_1 \rightarrow 0} \int_{C_1} H_d \cdot dl = \frac{1}{Z_0} \lim_{C_1 \rightarrow 0} \int_{C_1} E_s \cdot dl \quad (2.12)$$

where  $Z_0$  is the intrinsic impedance of the surrounding medium. Substituting (2.9) and (2.8) in

---



---

(2.11) yields

$$V_d = \frac{Z_0}{2} I_s \quad (2.13)$$

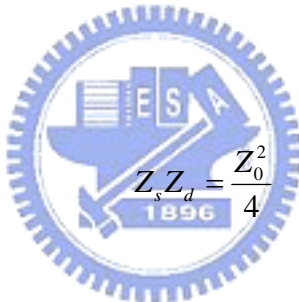
Substituting (2.10) and (2.7) in (2.12) yields

$$V_s = \frac{Z_0}{2} I_d \quad (2.14)$$

Multiplying (2.13) and (2.14) we obtain

$$\frac{V_s}{I_s} \frac{V_d}{I_d} = \frac{Z_0^2}{4} \quad (2.15)$$

or



$$Z_s Z_d = \frac{Z_0^2}{4} \quad (2.16)$$

Thus, we get Booker's result that the terminal impedance  $Z_s$  of a slot antenna is equal to 1/4 of the square of the intrinsic impedance of the surrounding medium divided by the terminal impedance  $Z_d$  of the complementary dipole antenna. Infinite, flat, and very thin conductors are not realizable in practice but can be closely approximated. If a slot is cut into a plane conductor that is large compared to the wavelength and the dimensions of the slot, the behavior predicted by *Babinet's principle* can be realized to a high degree. The impedance properties of the slot may not be affected as much by the finite dimensions of the plane as would be its pattern. The slot shown in Fig. 2.2 will radiate on both sides of the screen. Unidirectional radiation can be obtained by placing a backing (box or cavity) behind the slot, forming a so-called *cavity-backed slot* whose radiation properties (impedance and pattern) are determined by the dimensions of the cavity.

2.1.3 Patterns of Slot antennas

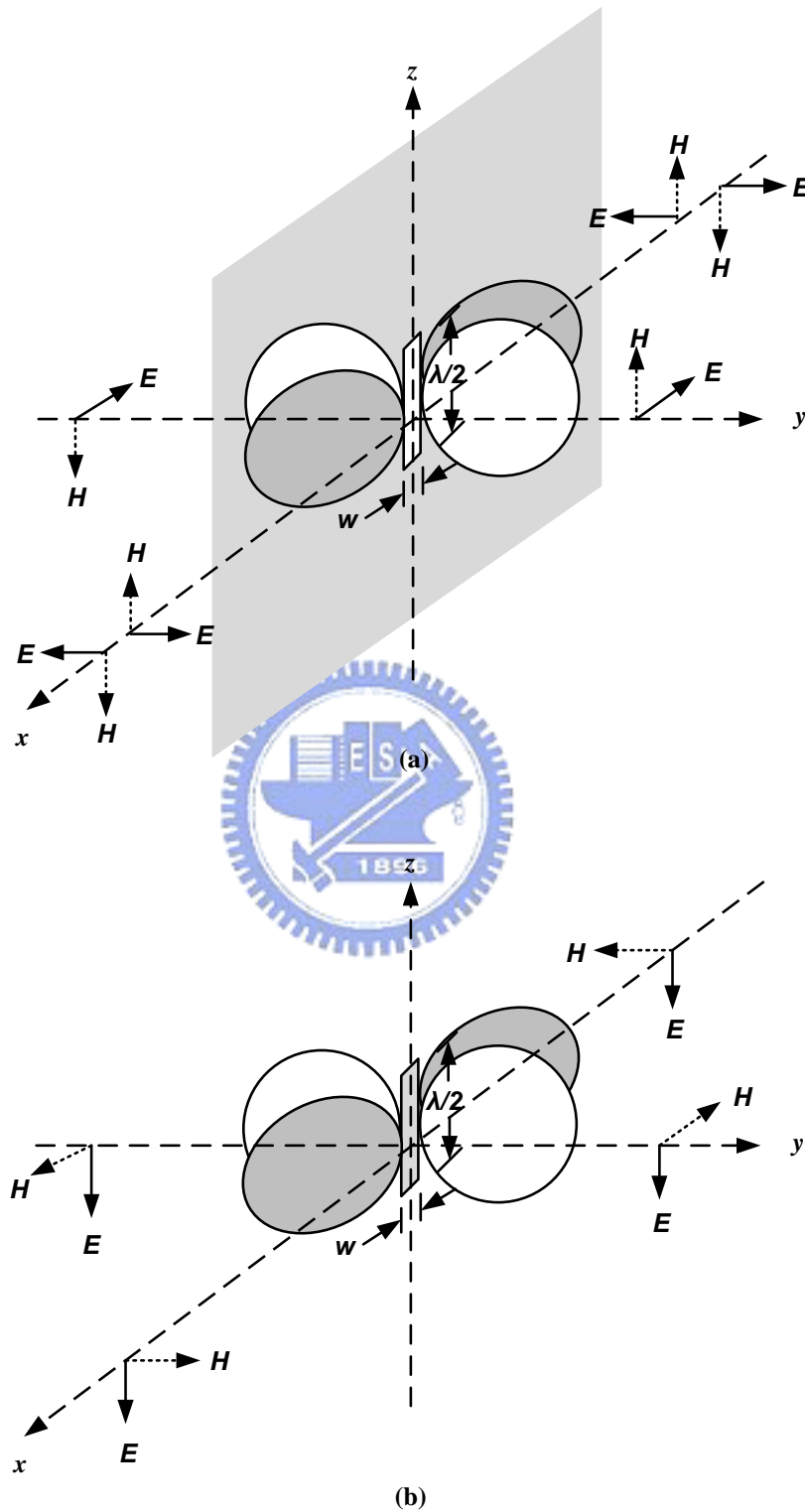


Fig. 2.3 Radiation fields of a (a)  $\lambda/2$  slot on a screen and (b) a  $\lambda/2$  flat dipole.

The slot of Fig. 2.2 can be made to resonate by choosing the dimensions of its complement (dipole) so that it is also resonant. The pattern of the slot is identical in shape to that of the dipole except that the **E**- and **H**-fields are interchanged. When a vertical slot is mounted on a vertical screen, as shown in Fig. 2.3(a), its electric field is horizontally polarized while that of the dipole is vertically polarized [Fig. 2.3 (b)]. Changing the angular orientation of the slot or screen will change the polarization.

The slot antenna, which is a cavity-backed design, has been utilized in a variety of law enforcement applications. Its main advantage is that it can be fabricated and concealed within metallic objects. There are various methods of feeding a slot antenna. For proper operation, the cavity depth must be equal to odd multiples of  $\lambda_g/4$ , where  $\lambda_g$  is the guide wavelength.

#### 2.1.4 Microstrip-to-slot Cross-Junction Transition

The transition has been comprehensively analyzed by many investigators. A layout of this transition is shown in Fig. 2.4.

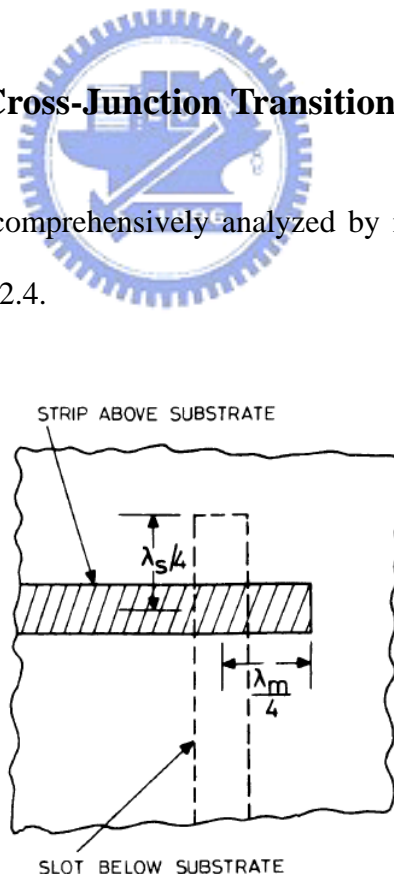


Fig. 2.4 Microstrip-to-slot transition

A transmission line equivalent circuit of the transition (Fig. 2.4) proposed by *Chambers* is shown in Fig. 2.5. The reactance  $X_{0s}$  represents the inductance of a shorted slot, and  $C_{0c}$  is the capacitance of an open microstrip.  $Z_{0s}$  and  $Z_{0m}$  are the slot and microstrip characteristic impedance respectively.  $\theta_s$  and  $\theta_m$  represent the electrical lengths (quarter-wave at the center frequency) of the extended portions of the slot and the microstrip, respectively, measured from the reference planes as shown in Fig. 2.5. The transformer turns ratio  $n$  represents the magnitude of the coupling between the microstrip and slot.

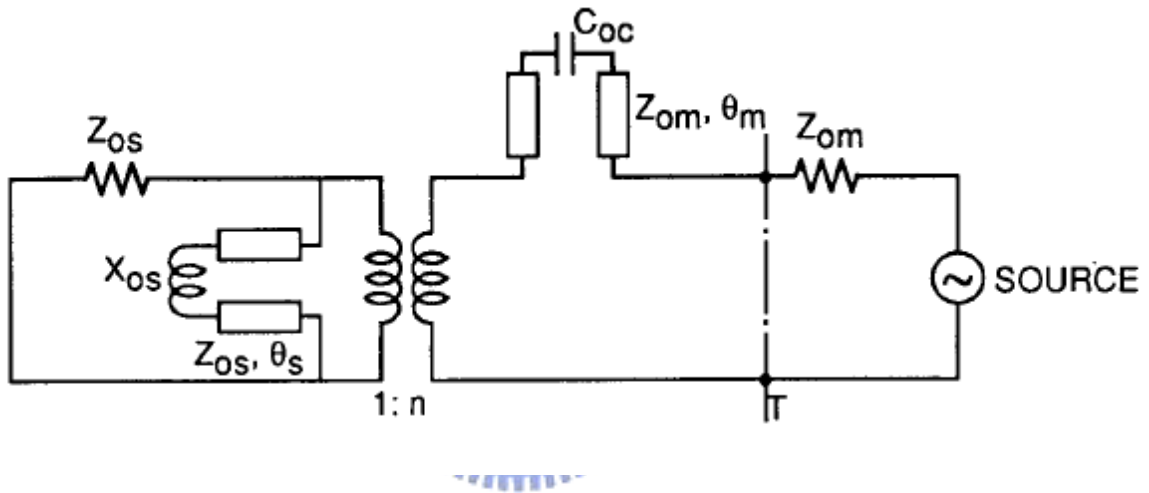


Fig. 2.5 Transmission line equivalent circuit for the transition of Fig. 2.4

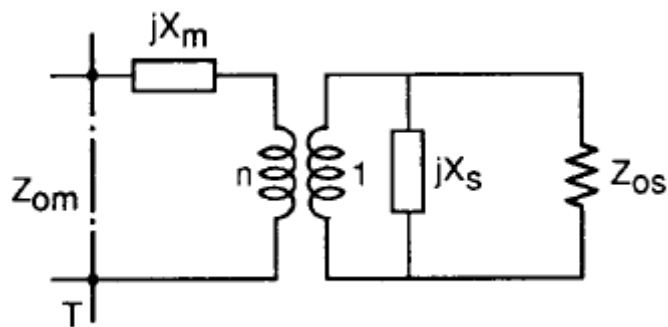


Fig. 2.6 Reduced equivalent circuit of Fig. 2.5

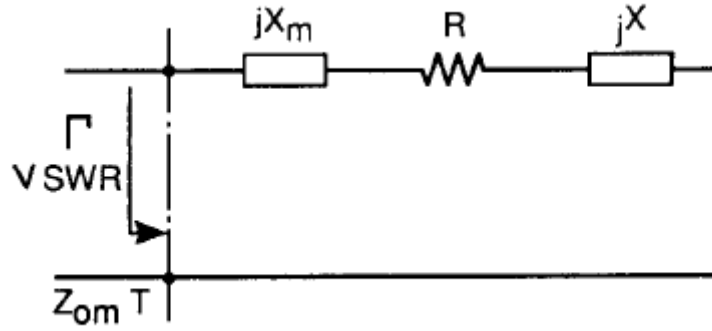


Fig. 2.7 Transformed equivalent circuit of Fig. 2.6

For further analysis the equivalent circuit in Fig. 2.5 may be redrawn as in Fig. 2.6. Here,

$$jX_s = Z_{0s} \frac{jX_{0s} + jZ_{0s} \tan \theta_s}{Z_{0s} - X_{0s} \tan \theta_s} \quad (2.17)$$

and

$$jX_m = Z_{0m} \frac{1/j\omega C_{0c} + jZ_{0m} \tan \theta_m}{Z_{0m} + \tan \theta_m / \omega C_{0c}} \quad (2.18)$$

After transformation to the microstrip side, the equivalent circuit of Fig. 2.6 reduces to that shown in Fig. 2.7. In this circuits,

$$R = n^2 \frac{Z_{0s} X_s^2}{Z_{0s}^2 + X_s^2} \quad (2.19)$$

and

$$X = n^2 \frac{Z_{0s}^2 X_s}{Z_{0s}^2 + X_s^2} \quad (2.20)$$

Finally, the reflection coefficient  $\Gamma$  is given by

$$\Gamma = \frac{R - Z_{0m} + j(X_m + X)}{R + Z_{0m} + j(X_m + X)} \quad (2.21)$$

From the above analysis, we can determine the characteristic impedance of the slot  $Z_{0s}$  to match the microstrip line impedance  $Z_{0m}$ .

## 2.2 High-Performance Techniques

In this section, we introduce a number of techniques that improve the performance along various dimensions: antenna size, impedance bandwidth, and so on.



### *A Novel Approach for Miniaturization of Slot Antennas [8]*

By utilizing the virtual enforcement of the required boundary condition (BC) at the end of a slot antenna, the area occupied by the resonant antenna can be reduced. To achieve the required virtual BC, the two short circuits at the end of the resonant slot are replaced by reactive BC, including inductive or capacitive loadings. By means of these loads, we can reduce the size of the resonant slot antenna for a given resonant frequency without adding any condition on the impedance matching of the antenna.

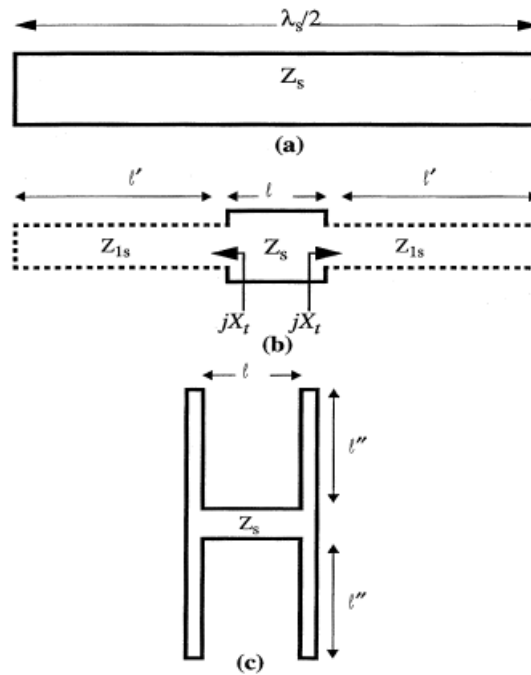


Fig. 2.8 Transmission line model of a slot antenna (a) half-wave slot antenna. (b) Inductively terminated slot antenna. (c) Two series inductive terminations

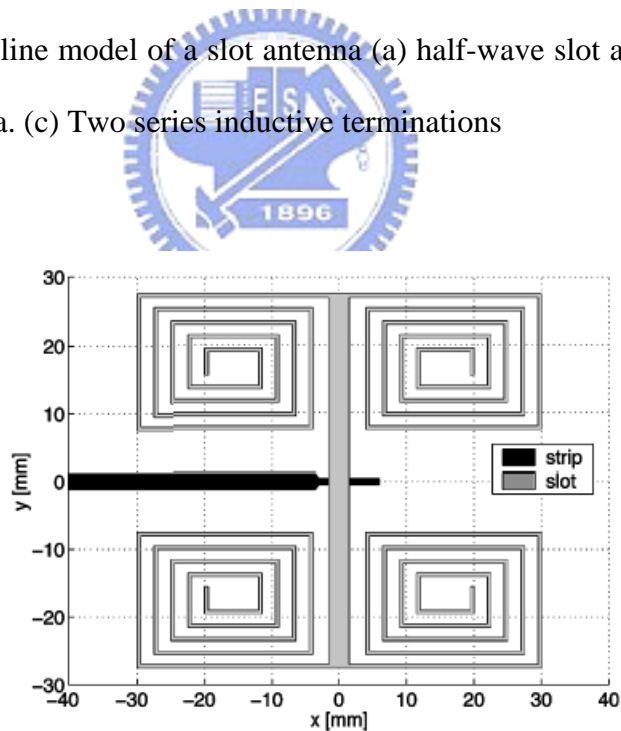


Fig. 2.9 The geometry of the antenna and its feed designed to operate at 300MHz

***A Wide-Band Slot Antenna Design Employing a Fictitious Short Circuit Concept [9]***

A resonant narrow slot antenna is equivalent to a magnetic dipole, and its first resonant



frequency corresponding to the electrical length of  $\lambda_g/2$  ( $\lambda_g/2$  is the guided wavelength in the slot). If the slot antenna is fed near an edge by a microstrip line and the slot width is properly chosen at a frequency above the first slot resonance, then a fictitious short circuit near the microstrip feed may be created. The reason is that the tangential component of the electric field created by the microstrip line at a particular distance cancels out the electric field of the slot excited by the return current on the ground plane of the microstrip line. When appropriately fed, these two resonances can merge and result in an antenna with a much larger bandwidth or two separate bands of operation with similar radiation characteristics.

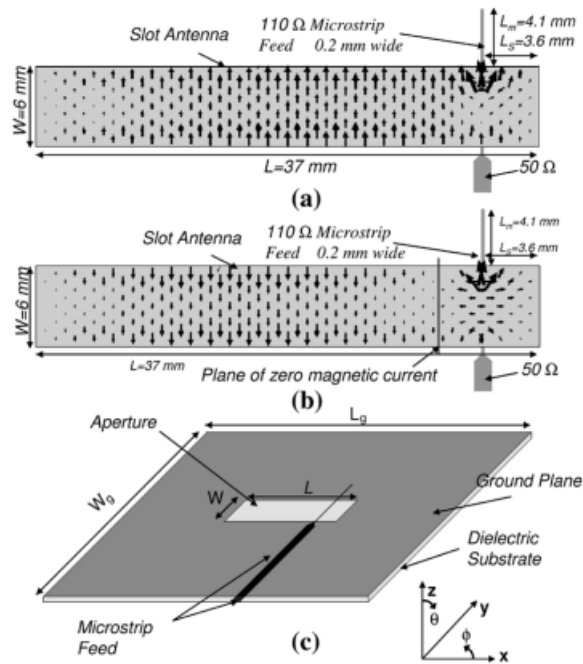


Fig. 2.10 Electric field distributions and three-dimensional geometry of a microstrip-fed slot antenna (a) Normal field distribution (b) Field distribution at a slightly higher frequency showing a fictitious short circuit along the slot causing the second resonance (c) Three-dimensional geometry

**Bandwidth Enhancement and Size Reduction of Microstrip Slot Antennas [10]**

The variation in the slot shape, from straight to L and T shapes, which generate

additional resonances when coupled to the original resonances of the slot, further increases impedance bandwidths. By suitably selecting the design parameters, the impedance bandwidths of up to 60% 84%, and 80% are achieved for these straight, L and inverted T slots, respectively.

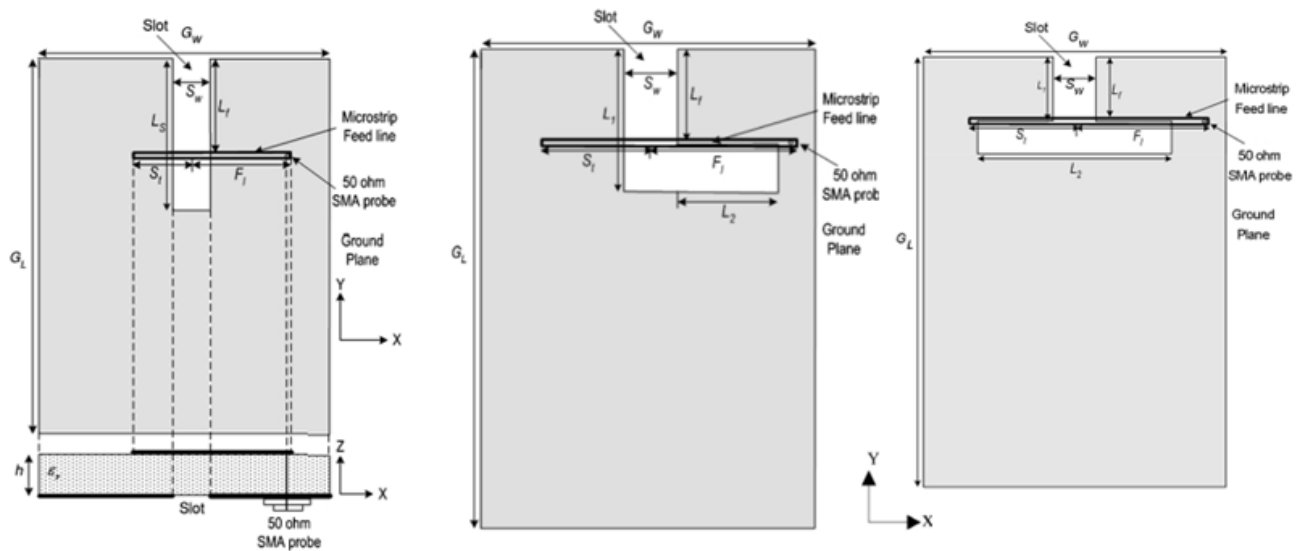


Fig. 2.11 Geometry of the straight, L and T shapes slot antennas



***Band-Rejected Design of the Printed Open Slot Antenna for WLAN/WiMAX Operation***

[11]

First, the broadband characteristic of open slot antenna design with small size is implemented and measured. Next, we insert a single strip on the broadband antenna. The dispensable band is rejected by inserting a metal strip on the open slot of the broadband antenna. Due to the metal of strip connected to the ground plane, the major current distribution will be concentrated on the strip and will produce a band-rejected function. The length of the inserting strip, which corresponds to quarter-wavelength, determines the center frequency of rejected band.

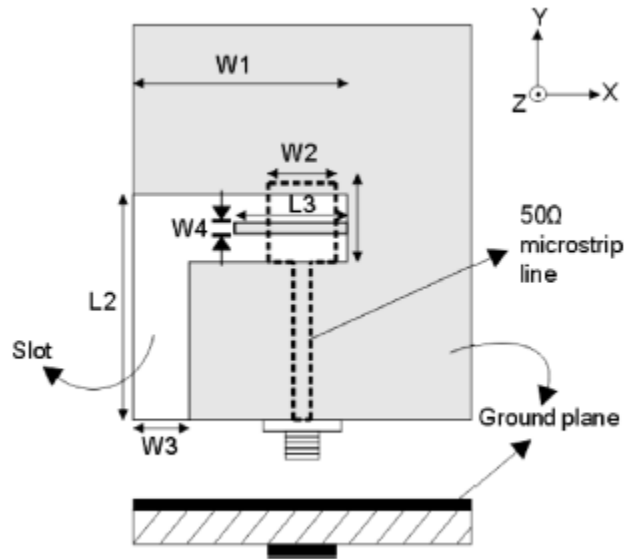


Fig. 2.12 Geometry of the band-rejected open slot antenna for WLAN bands

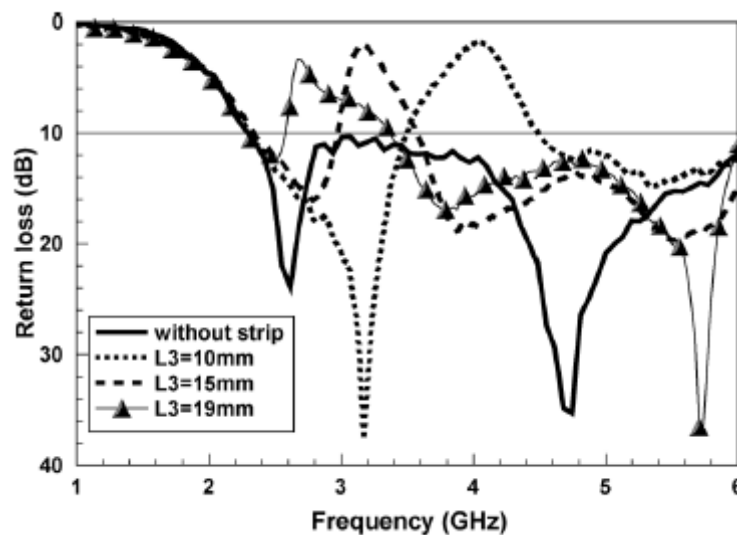


Fig. 2.13 Measured return loss for various lengths ( $L_3$ ) of the antenna

### ***Microstrip-Fed Slot Antennas with Suppressed Harmonics*** [12]

As shown in Fig. 2.14, the rectangular slot type harmonic suppressed antenna is composed of the conventional rectangular slot antenna and a double spur-line in the rectangular slot connected with ground plane to achieve wide-band harmonic suppression. Conductor line ( $L_{cl}$ ) and the gap ( $W_{cl}$ ) between conductor line and ground plane can be modeled as a shunt-series resonator ( $L_s$ - $C_s$ ) with wide-bandstop characteristic over the second

and third harmonic frequencies, and its equivalent circuit can be inserted inside the slot radiator as shown in Fig. 2.13(d).

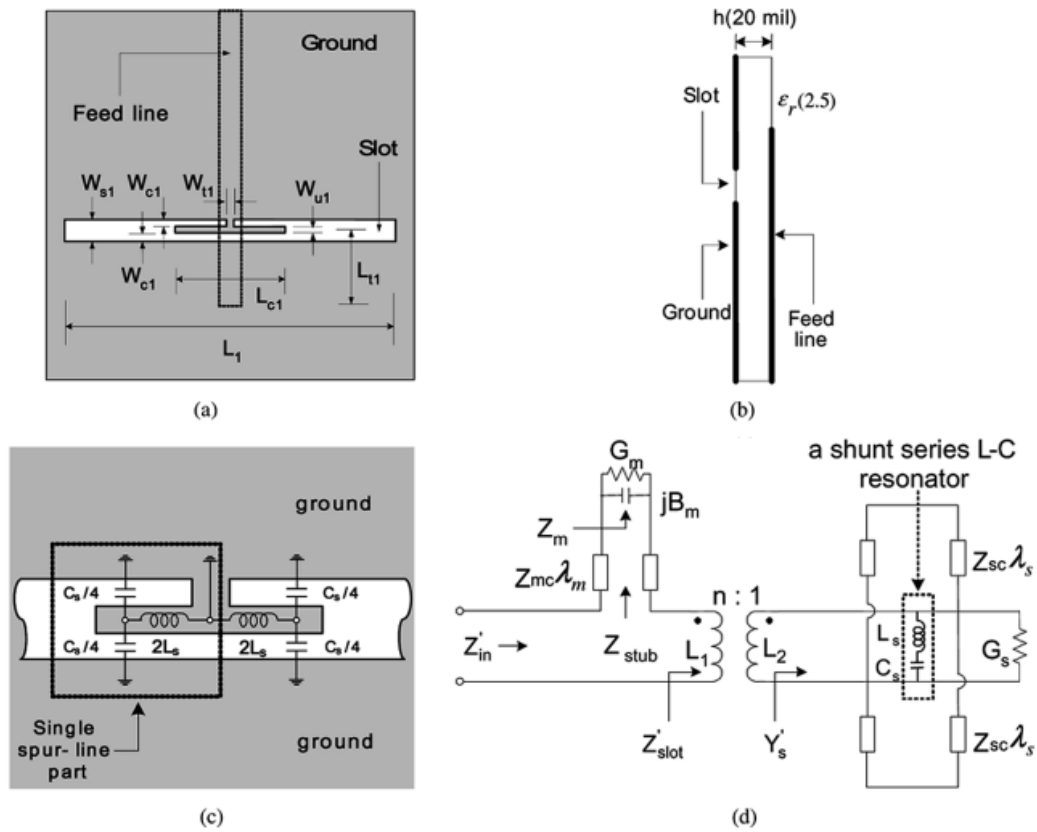


Fig. 2.14 (a) Top view, (b) side view, (c) limped-element equivalent circuit model for the rectangular slot type radiator, and (d) total equivalent circuit of the rectangular slot type harmonic suppressed antenna

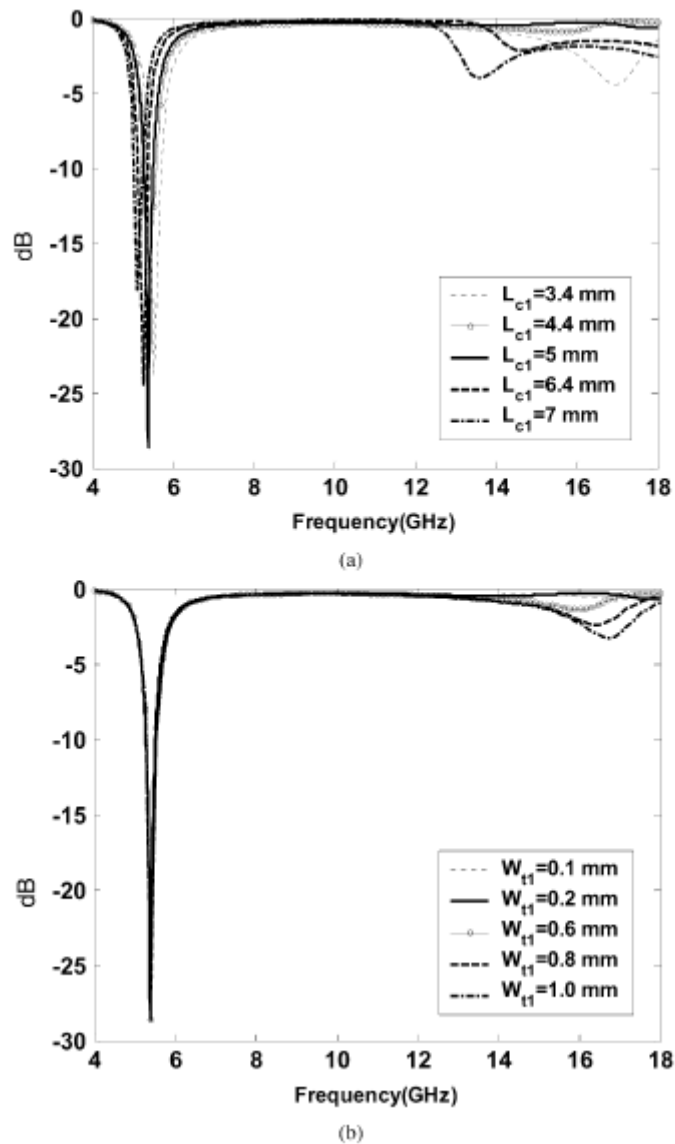


Fig. 2.15 Simulated return losses for (a) L and (b) W of the rectangular slot type HAS

### *Multiband Printed Monopole Slot Antenna for WWAN Operation in the Laptop Computer*

[3]

The antenna is formed by three slots operated at their quarter-wavelength modes and arranged in a compact planar configuration. A step-shaped microstrip feedline is used to excite the three monopole slots at their respective optimal feeding position, and two wide operating bands at about 900 and 1900 MHz are obtained for the antenna to cover all the five

operating bands of GSM850/900/1800/1900/UMTS for WWAN operation.

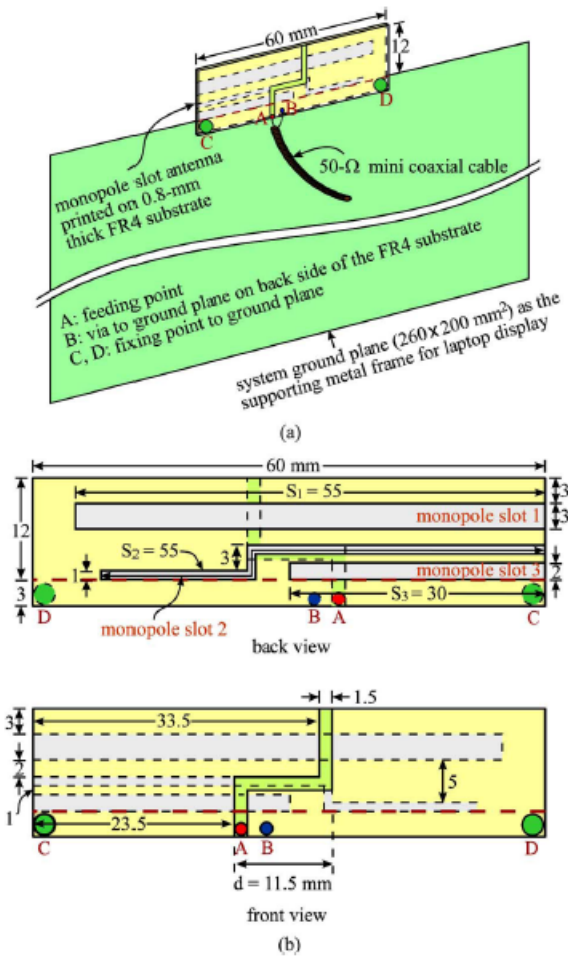


Fig. 2.16 (a) Geometry of the multiband printed monopole slot antenna for WWAN (wireless wide area network) operation in the laptop computer (b) Dimensions of the antenna

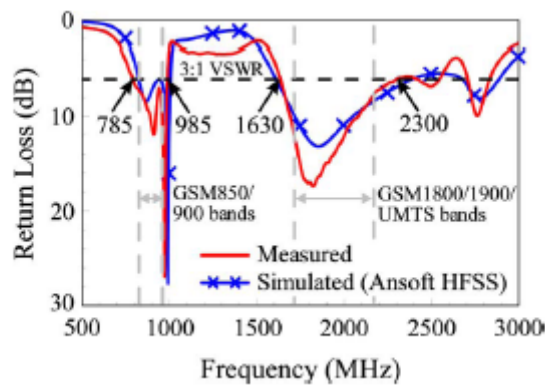


Fig. 2.17 Measured and simulated return loss for the proposed antenna

## **Chapter 3      Review of Multiband Antennas for Mobile Phones**

---

### **3.1 Literature Review**

Modern mobile phone is required to operate multiband to satisfy various communication services. The demand of compact, light weight, reduced height, and multifunctional mobile phones is a challenge to antenna designers. Novel antenna designs are needed to meet the requirements of these emerging trends in mobile communication. In this chapter, we discuss some multiband antennas for mobile phone applications as follows.

The internal multi-resonant monopole antenna is designed for GSM900/DCS1800/US-PCS/S-DMB band and is shown in Fig 3.1. The multi-resonant operation of the antenna is achieved by utilizing a bent tuning stub, a shorting strip line, a U-shaped slit and the addition of a narrow resonant slit to the main radiator. The first resonant frequency is excited by the main radiator of the antenna, and the second resonant frequency is controlled by the length of the bent tuning stub. Finally, the third resonant frequency is generated by adding a narrow resonant slit to the perimeter of the main radiator. Hence, the resonant frequencies of the antenna can be independently controlled by tuning the length of the individual elements of the antenna. The dimensions of the main radiator are obtained using

$$f_0 = \frac{c}{4(W + L)} \quad (3.1)$$

where  $c$  is the speed of light in free space,  $f_0$  is the desired resonant frequency,  $W$  and  $L$  are the width and length of the main radiator.

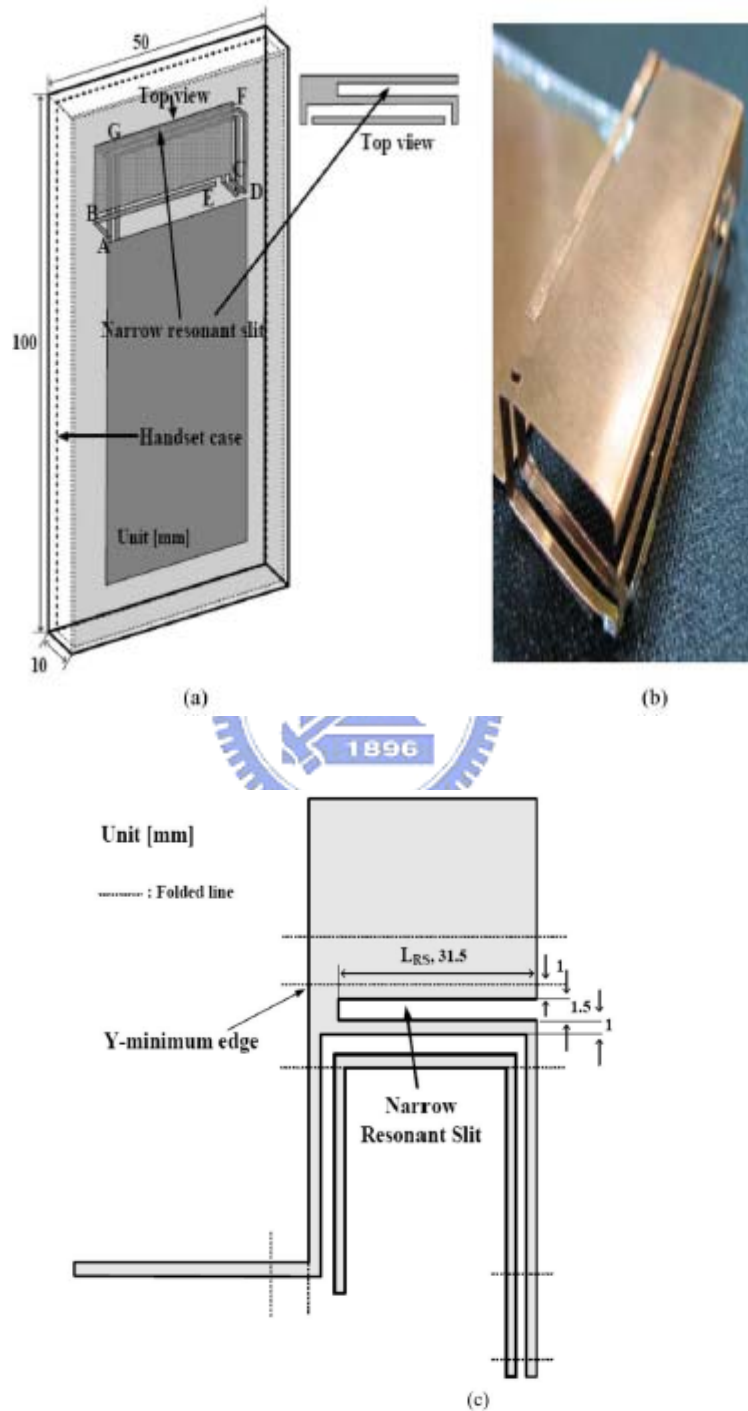


Fig. 3.1 Geometry of the triple-band antenna (a) 3-D view, (b) fabricated internal monopole antenna, (c) unfolded structure of radiating elements



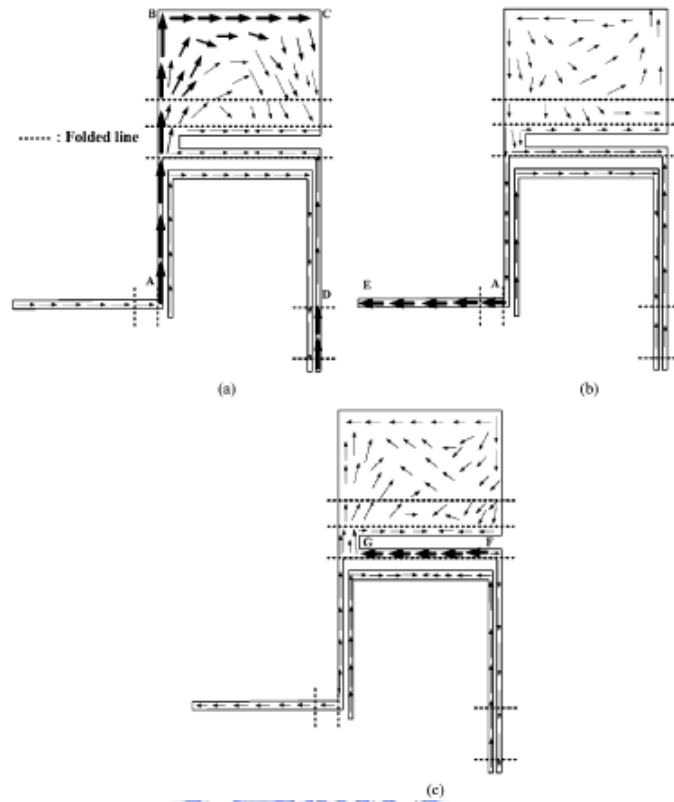


Fig. 3.2 Surface current distributions on the radiating elements for triple-resonant antenna: (a) 930 MHz, (b) 1850 MHz, (c) 2630 MHz

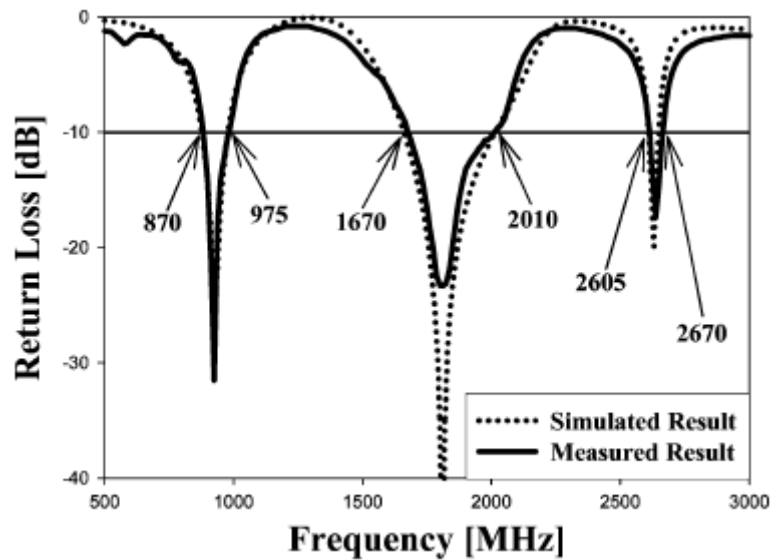


Fig. 3.3 Comparison between measured and simulated results of triple-resonant antenna

The compact multiband folded loop chip antenna is present in [16]. The loop antenna can be seen as a chip antenna to be surface-mountable on the system circuit board. However, unlike above discussions, the first resonant mode of the multiband loop antennas for mobile phone applications is a 0.5-wavelength resonant mode instead of quarter-wavelength resonant mode. The antenna has a simple metal pattern comprising a folded loop strip and a tuning pad, and is suited for application in small-size mobile phones (ground plane length 60 mm only). The metal pattern is attached on the surfaces of a foam base, and the first three resonant modes (0.5-, 1.0-, and 1.5-wavelength modes) of the antenna can be excited with good impedance matching by simply adjusting proper dimensions of the tuning pad and its location along the folded loop strip.

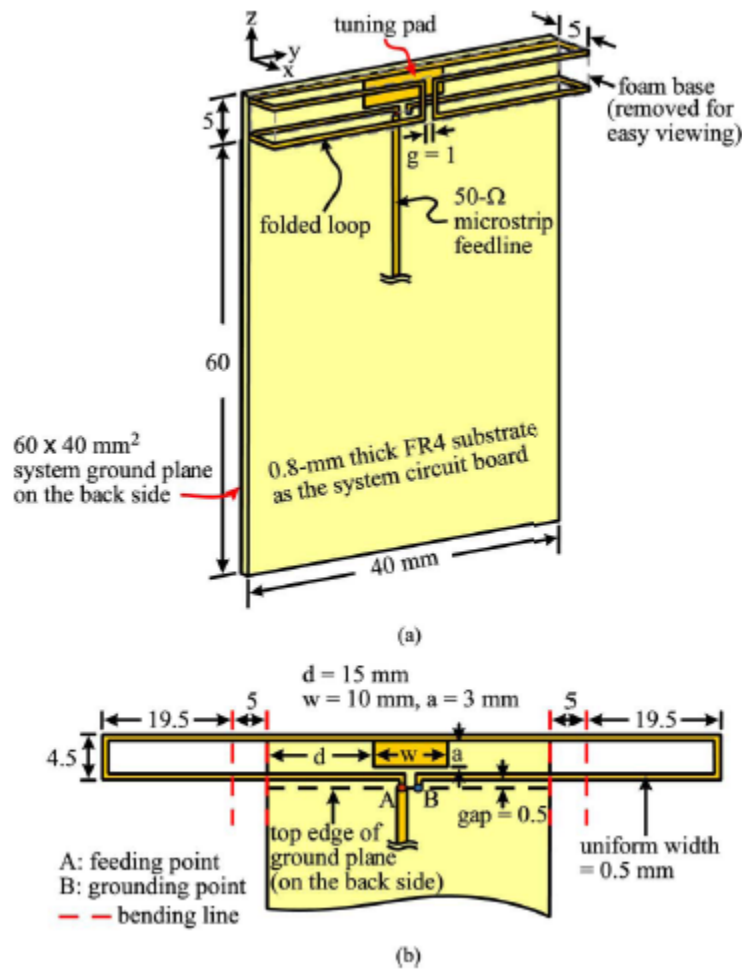


Fig. 3.4 (a) Geometry of the proposed folded loop chip antenna (b) Detailed dimensions of the antenna unfolded into a planar structure

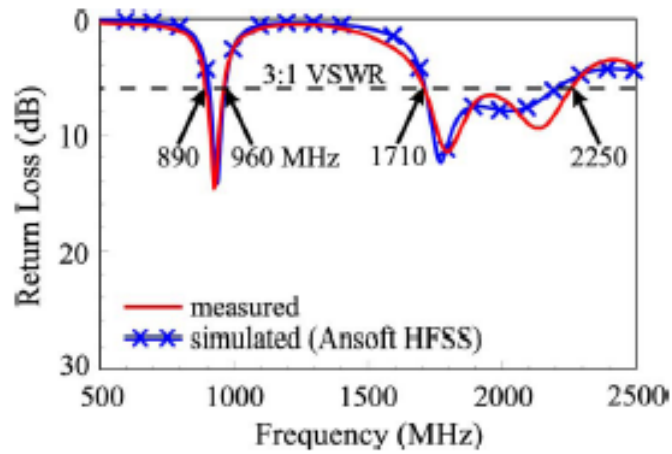


Fig. 3.5 Measured and simulated return loss for the proposed antenna

The Hepta-band internal antenna is designed for personal communication application [15]. The antenna consists of a basic PIFA radiator, an L-patch located beneath the PIFA element and directly connected to the feed pin and an additional resonating strip for operation in WLAN band around 5.2 GHz.

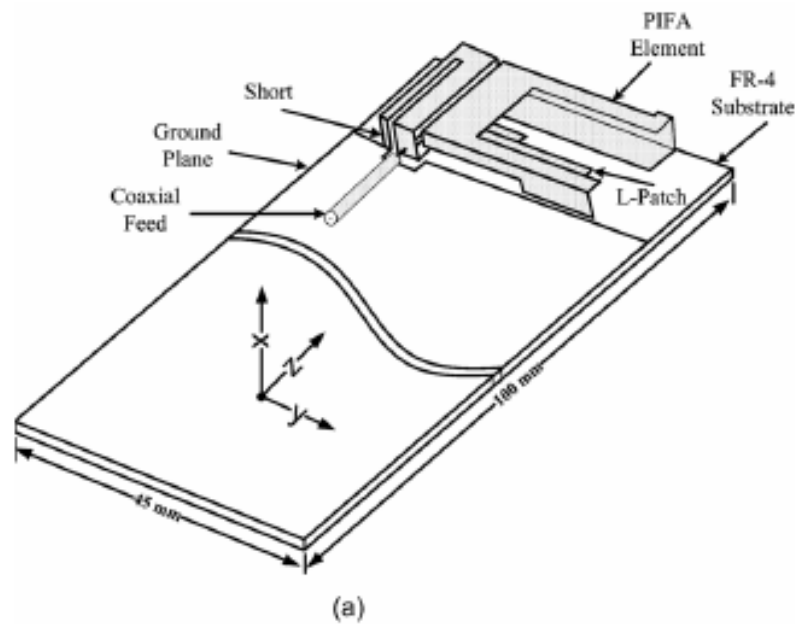


Fig. 3.6 Geometry of the antenna

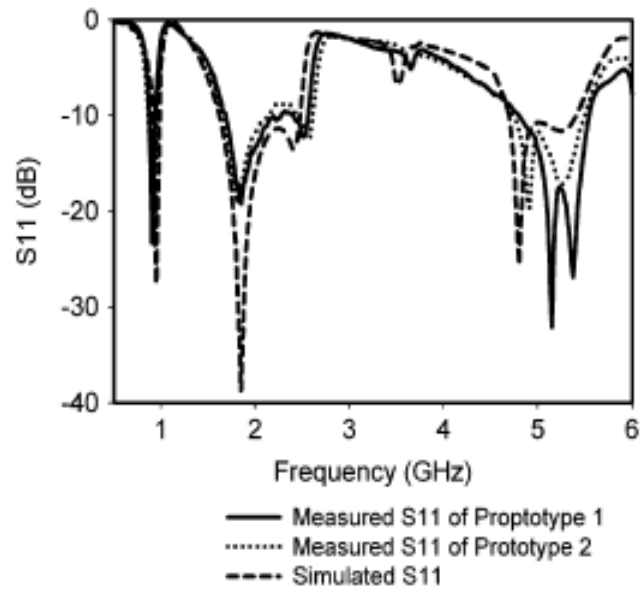


Fig. 3.7 Comparison between the measured and simulated return losses

The printed monopole multiband slot antenna is present in [2]. The slot antenna consists of two slots of different lengths cut at the edge of the ground plane, which are excited by a  $50\text{-}\Omega$  microstrip feed line. Slot 1 has a longer length  $S_1$  and controls the excitation of the antenna's lower band, while the slot 2 has a shorter length  $S_2$  and controls the excitation of the antenna's lower band. The lengths are about one-quarter wavelength at 900 and 2100 MHz, respectively. Note that the two slots are chosen to have a wide width of 5mm ( $w_1$  and  $w_2$ ), which is helpful for widening the bandwidths for the antenna's lower and upper bands.

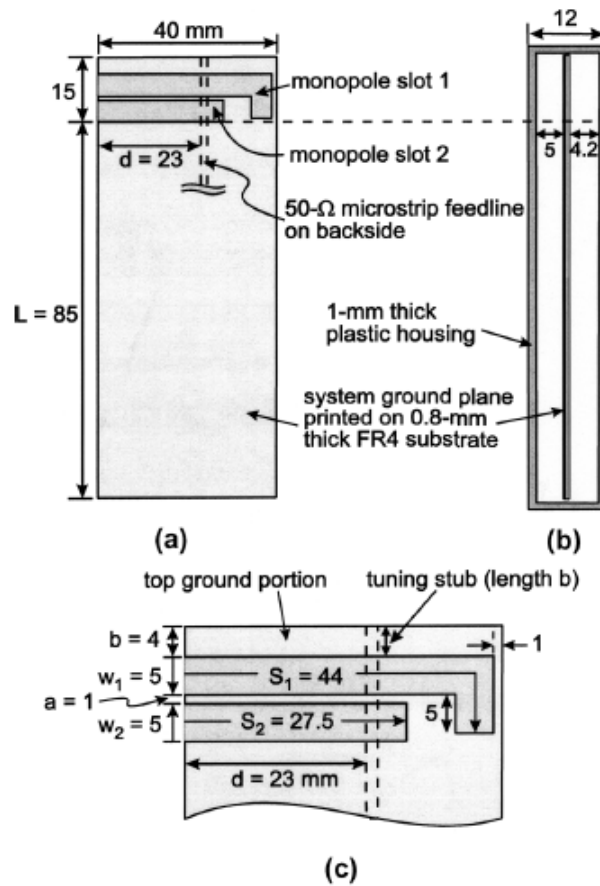


Fig. 3.8 (a) Geometry of the proposed printed monopole slot antenna for mobile phone application (b) Side view of the geometry in (a) with a 1-mm-thick plastic housing (c) Detailed dimensions of the antenna.

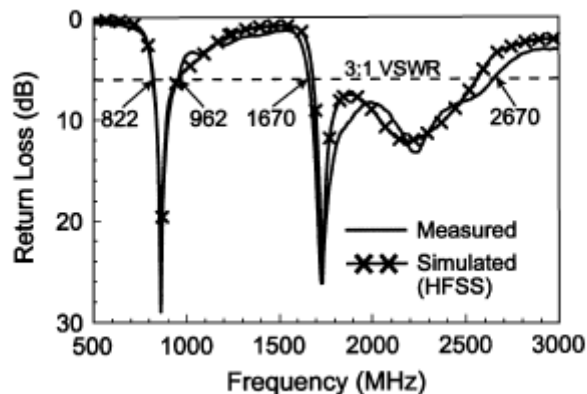


Fig. 3.9 Measured and simulated return loss for the antenna; the 1-mm-thick plastic housing is included

In conclusion, we list Table 3.I to compare the advantages and disadvantages of the above multiband antennas.

	Advantages	disadvantages
Monopole	Low profile.	It needs an enough large ground plane.
Loop	Multiband is achieved by utilizing only one resonant path.	It comprises a folded loop strip attached on a foam base, which is difficult to fabricate.
PIFA	Reduce antenna area.	Narrow bandwidth and larger thick due to shorting pin (5-10mm).
Slot	It is suitable to be printed on the system circuit board, and low profile, low cost.	Higher band may be affected by the ground plane size.

Table 3.I Comparison of various multiband antennas

In my opinion, the advantages of the slot antenna outweigh its disadvantages from Table 3.I.

Hence, we select the slot antenna as our approach to multiband antenna.

## Chapter 4 The Proposed Slot Antenna

---

### 4.1 Antenna Configuration and Operation

Fig. 4.1 shows the geometry of the proposed printed slot antenna for mobile phone applications. The antenna is printed on the top portion of the system circuit board of the mobile phone, whose dimensions are selected to be 60 mm in length and 35 mm in width. The selected dimensions are reasonable for general mobile phones, and in this study the circuit board is fabricated using a 0.8-mm-thick FR4 substrate of relative permittivity 4.4 and loss tangent 0.02. The printed metal on the FR4 substrate has a conductivity of  $5.8 \times 10^7 \text{ S/m}$ . A  $50 \Omega$  microstrip feedline is used in this antenna design to excite two L-shaped slots on the ground in order to generate two bands, respectively. The longer slot ( $L_1+L_2+L_3$ ) controls the excitation of the lower band centered at about 900MHz to cover the GSM operation (890-960MHz), while the shorter slot ( $L_5+L_6$ ) controls the excitation of the upper band centered at about 2100MHz to cover the DCS/PCS/UMTS/WLAN/WiMAX operation (1710-2600MHz), which correspond to quarter-wavelengths at their resonant frequencies, respectively. Finally, the straight parasitic strip ( $L_p$ ), which is about half-wavelength of the WLAN band (5150-5350MHz), is electromagnetically coupled and excited by the shorter slot. The detailed antenna design parameters are listed in Table 4.I.

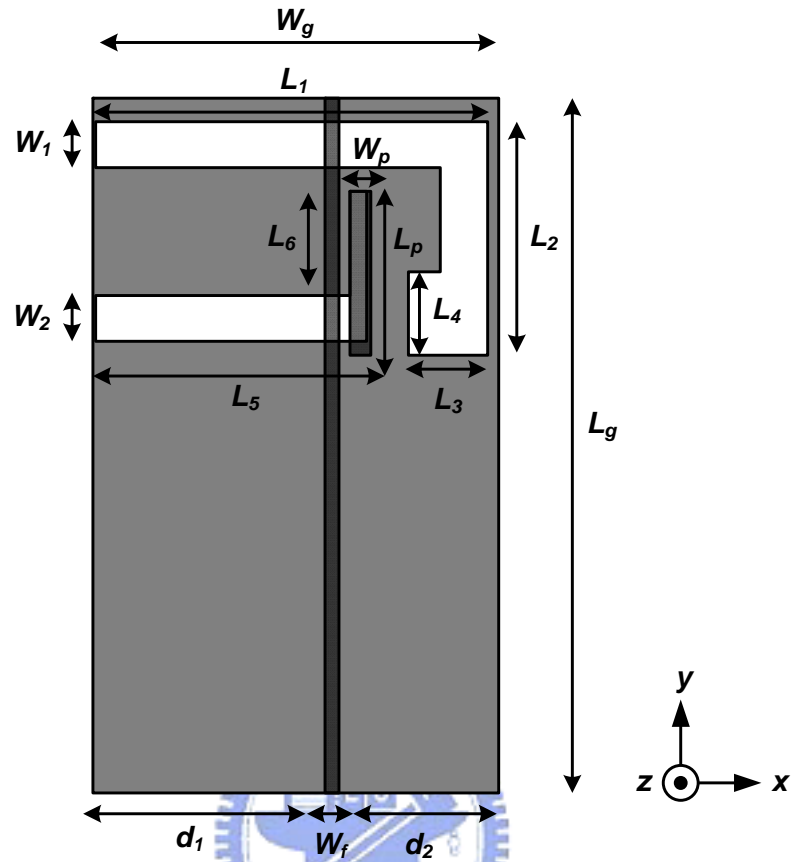
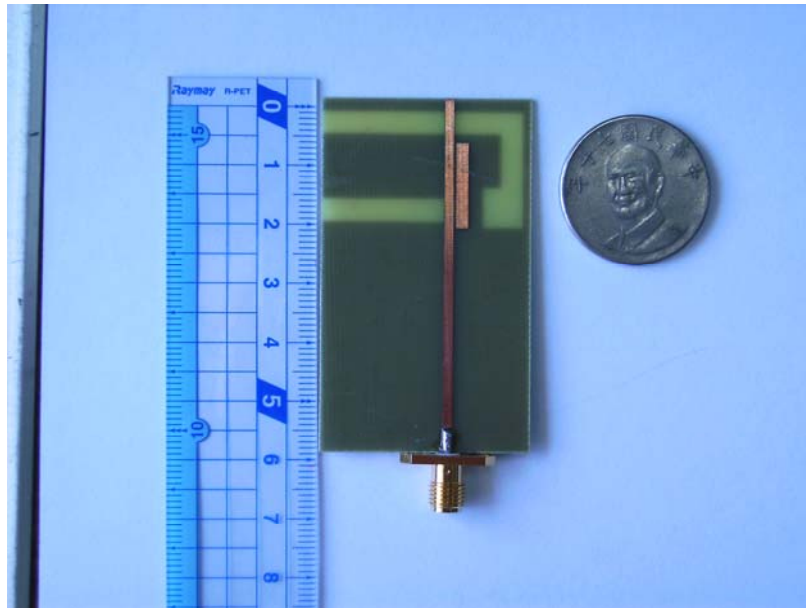


Fig. 4.1 Geometry of the proposed printed slot antenna

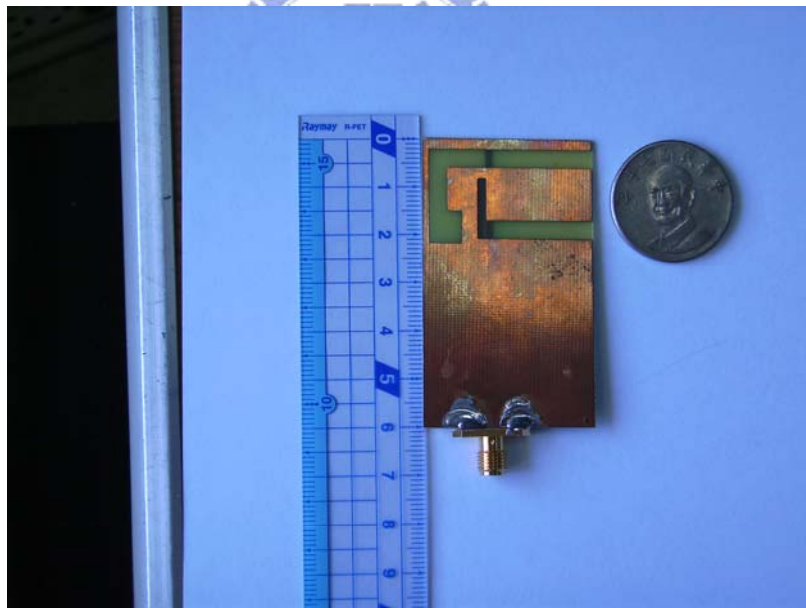
$W_g$	$L_g$	$W_f$	$d_1$	$d_2$
35	60	1.5	20	13.5
$W_1$	$W_2$	$L_1$	$L_2$	$L_3$
4	4	34	20	7
$L_4$	$L_5$	$L_6$	$W_p$	$L_p$
7	24	9	2	14.5

Table 4.1 Design Parameters (Unit: mm)





(a)



(b)

Fig. 4.2 Photographs of the fabricated antenna (a) top view (b) back view

## 4.2 Design Considerations and Procedure

To demonstrate the operation of the proposed antenna, Fig.4.3-4.6 performs the current distribution of each operation bands.

### A. GSM (890-960MHz) operation

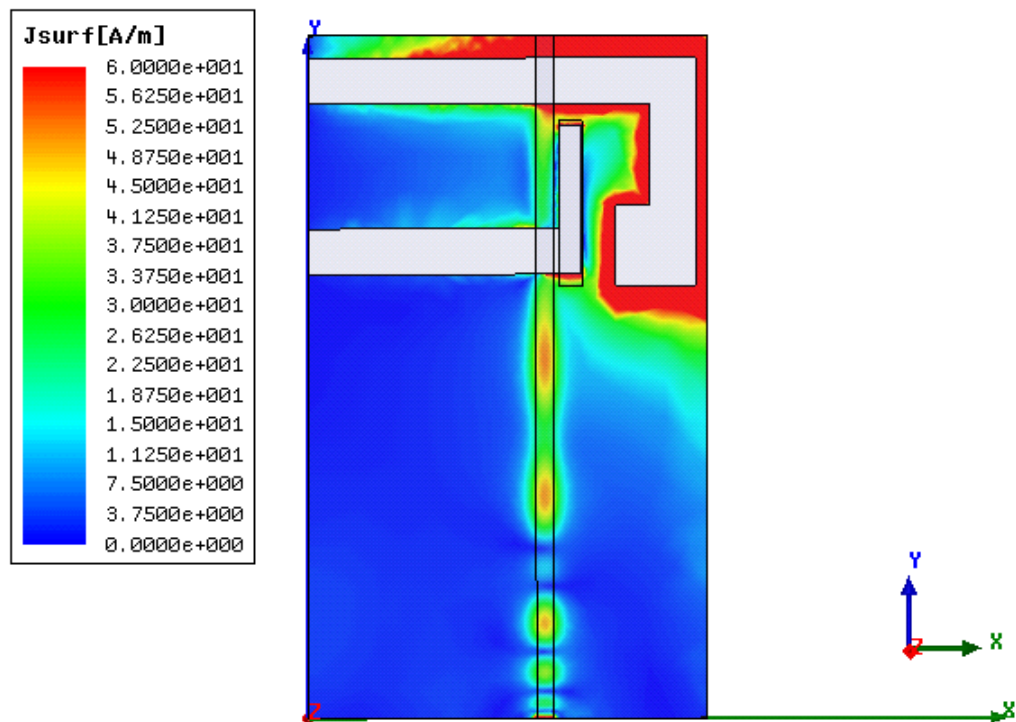


Fig. 4.3 Surface current distribution at 900MHz

First of all, in order to generate the GSM band, a  $50\Omega$  microstrip feedline printed at the location of  $d_1 = 20$  mm away from the edge of the ground plane excites the longer slot ( $L_1+L_2+L_3$ ), which is about quarter-wavelength at 900MHz.

*B. DCS/PCS/UMTS/WLAN/WiMAX (1710-2600MHz) operation*

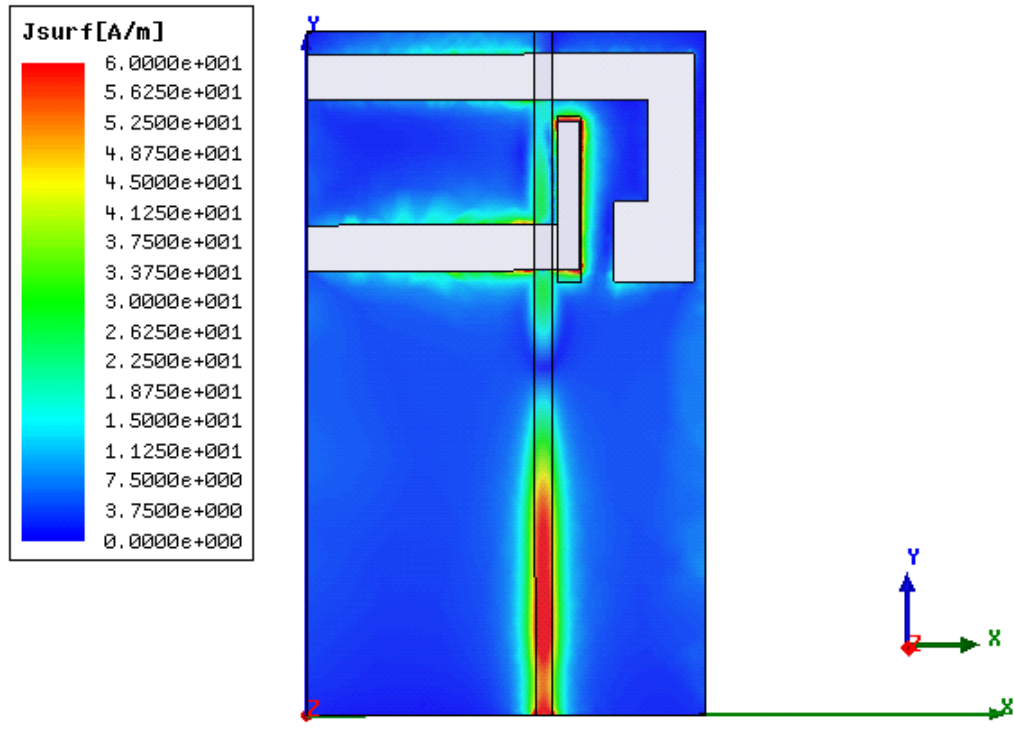


Fig. 4.4 Surface current distribution at 2100MHz

The shorter L-shaped slot ( $L_5+L_6$ ) helps in generating additional resonances, which when coupled to the original resonances of the slot, further increases impedance bandwidth [9]. It shows that the two orthogonal arms of the slot act as separate and tightly coupled resonators and their mutual coupling displaces their resonances toward lower and higher end frequencies. This phenomenon enhances the bandwidth significantly. By using this property, we can cover broad bandwidth (1710-2600MHz) with this simple structure.

*C. WLAN (5150-5350MHz) operation*

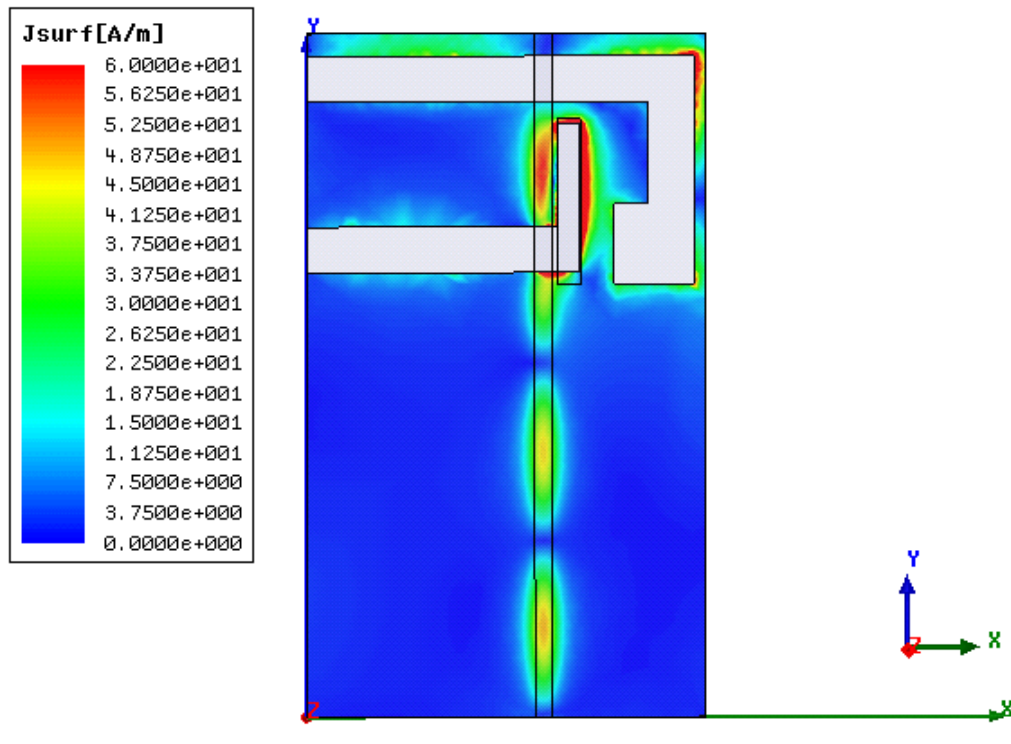


Fig. 4.5 Surface current distribution at 5200MHz

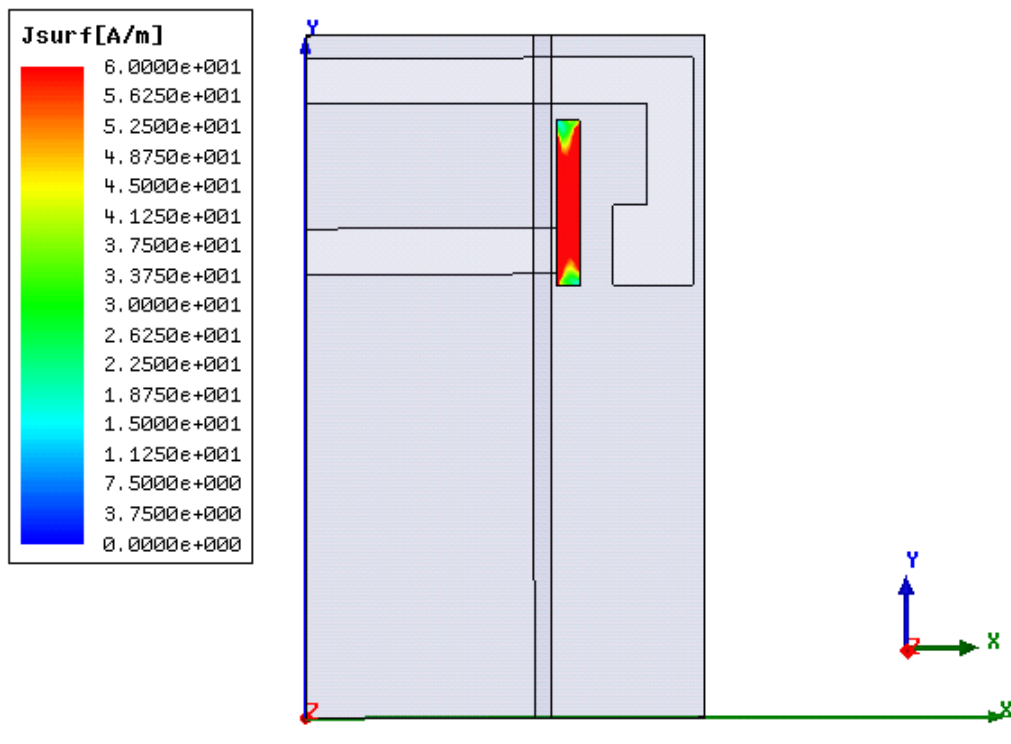


Fig. 4.6 Surface current distribution of the parasitic strip at 5200MHz

Finally, from Fig. 4.5 we can observe that the current distribution of the shorter slot at 5200MHz. In order to generate the WLAN band (5150-5350MHz) and mitigate the return loss degradation of other operating bands caused by the mutual coupling effect, we put a parasitic strip ( $L_p$ ) on the top portion above the shorter slot, which is about half-wavelength corresponding to 5.2GHz. The slots of ground which is the driven element electromagnetically couple and excite the parasitic strip controlling the operating frequency [12]. Thus, the parasitic strip is placed above the slot to generate the operating band, which increases the design freedom and possible applications.

### **4.3 Experimental Results and Discussions**

Fig. 4.7 shows the measured and simulated return loss of the proposed antenna. The simulated results are obtained from Ansoft simulation software High Frequency Structure Simulator (HFSS), and good agreement between the simulation and measurement is observed. In simulations, we used an ideal discrete port to excite the antenna. However, to test the prototype antennas, a coaxial cable is required to connect the antenna to the network analyzer. The feed cable being very close to the antenna while testing may affect the measurement results. Influence of the feed cable is more pronounced on the antenna radiation patterns as compared to the return loss. The proposed antenna generates the three bands centered at about 900, 2100 and 5200 MHz to cover the GSM/DCS/PCS/UMTS/WiMAX/WLAN bands, as shown in Fig.4.7.

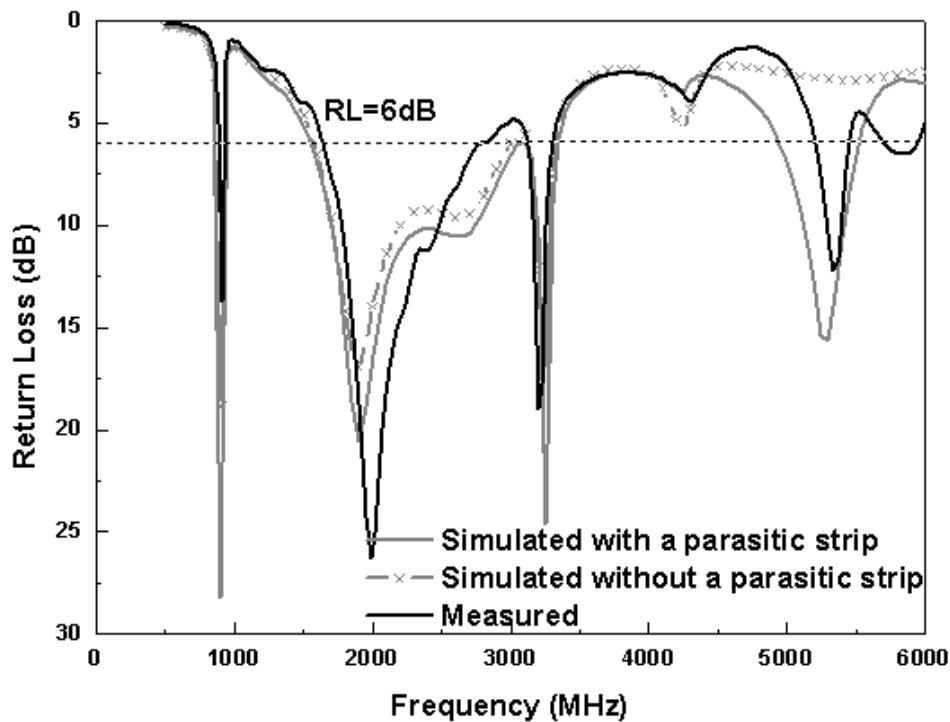


Fig. 4.7 Simulated and measured return loss for the proposed antenna

The proposed slot antenna is enclosed by a 1-mm-thick plastic housing, which is shown in Fig. 4.8. The material to simulate plastic cover for mobile phone is acrylonitrile butadiene styrene (ABS) with relative permittivity 3.5 and loss tangent 0.026. The simulated result shown in Fig. 4.9 indicates that the resonant frequencies of proposed antenna with a plastic housing are slightly lower compared with free space situation. The reason is because the effective permittivity is higher with a plastic housing. Hence, we can fine tune this antenna to satisfy a practical case easily.

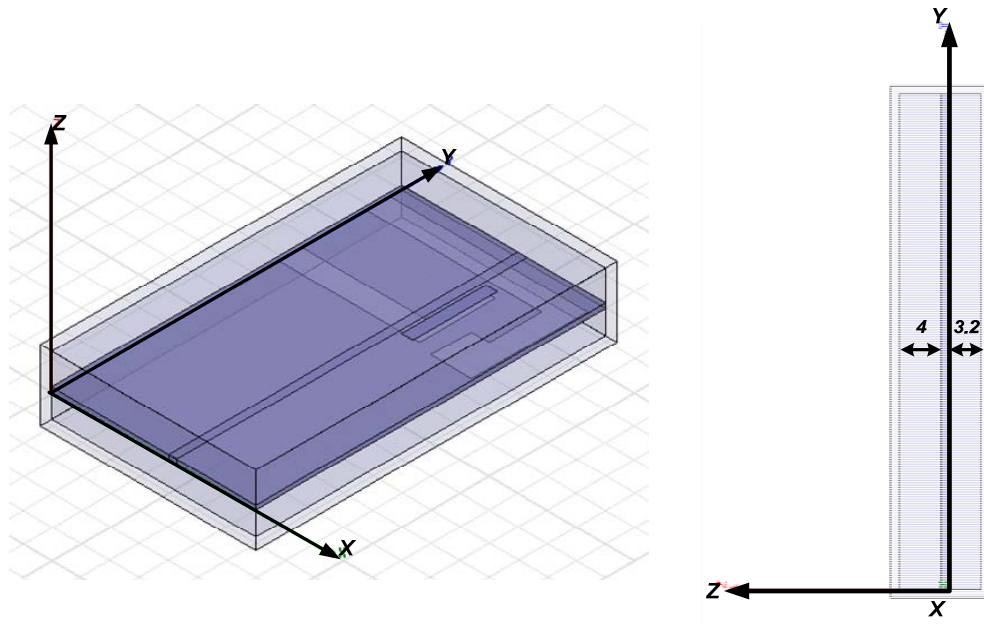


Fig. 4.8 Geometry of the proposed slot antenna with a 1-mm-thick plastic housing

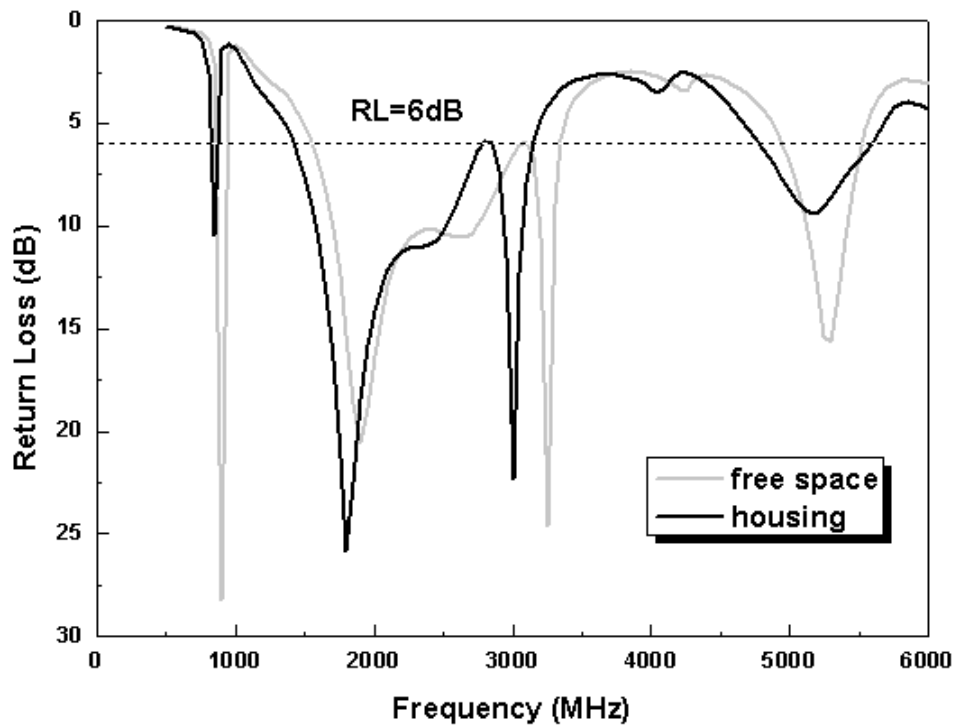


Fig. 4.9 Simulated return loss of the proposed antenna w/o plastic housing

When we consider the slot antenna of the mobile communication device for practical applications, the performances of the antenna will be significantly affected by the coupling effect of nearby electronic components. To study the effect of the nearby electronic components, we put a conducting box (PEC) of size  $33 \times 30 \times 6 \text{ mm}^3$  on the ground as a battery to simulate this case. The simulated result in Fig. 4.10 indicates that the performance of the proposed antenna is almost not affected. Thus, it becomes possible that the nearby electronic components can be placed in close proximity to the proposed antenna, with small effects on the performances of the antenna. This property indicates that the proposed slot antenna is EM compatible with the nearby electronic components.

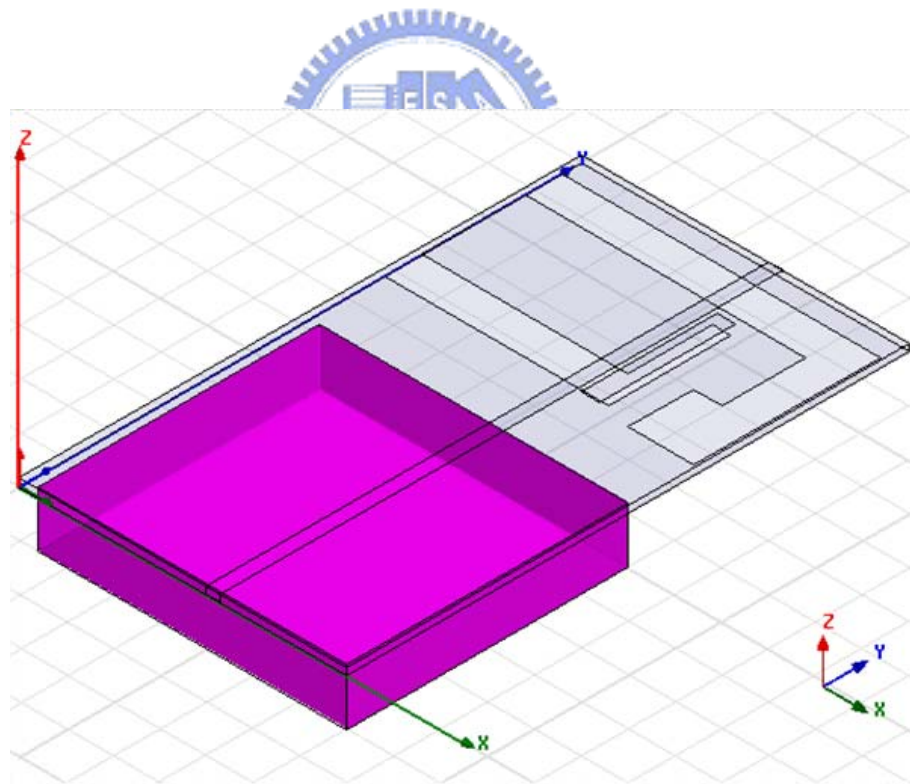


Fig. 4.10 A conducting box (PEC) of size  $33 \times 30 \times 6 \text{ mm}^3$  on the ground is used to simulate the battery case



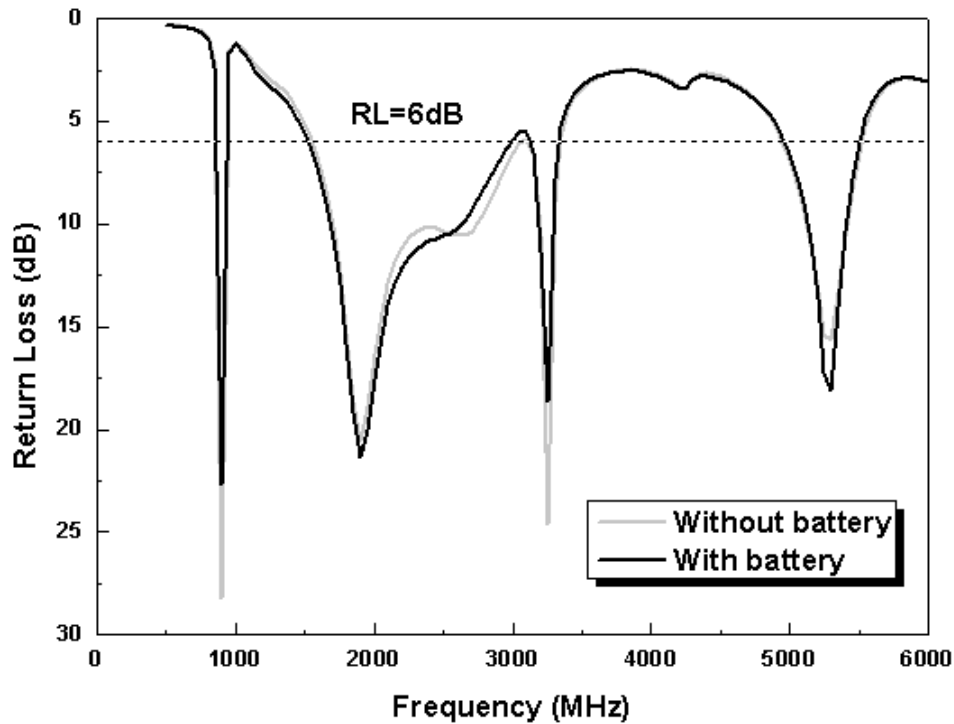
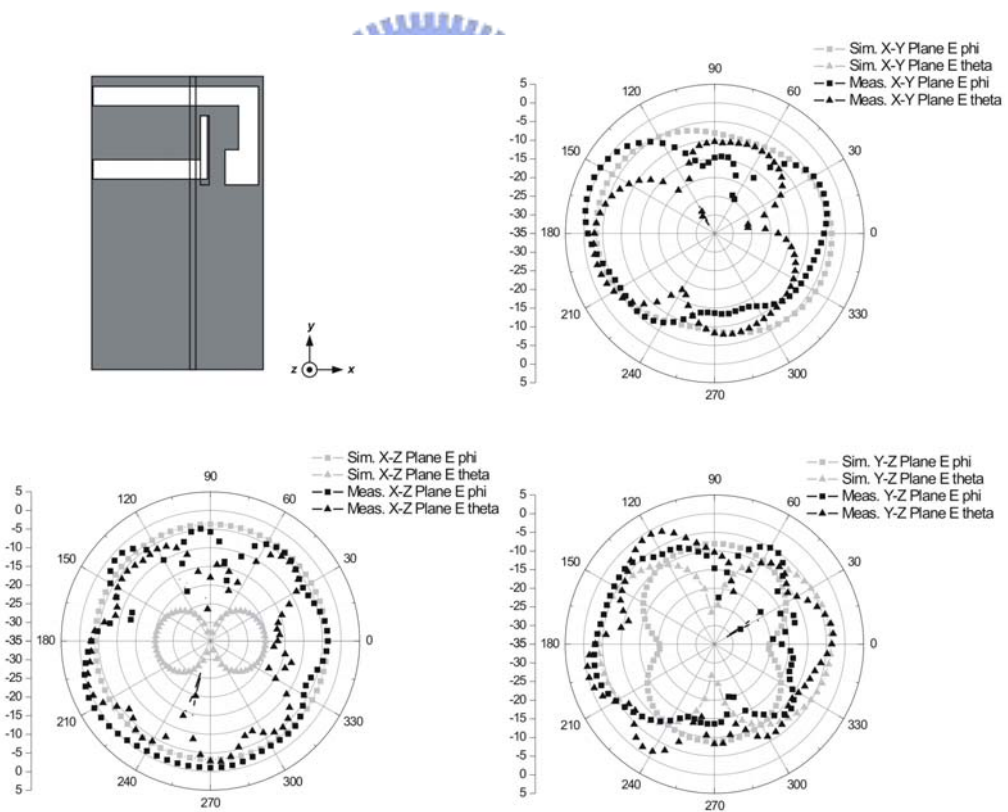


Fig. 4.11 Simulated return loss of the proposed antenna with and without a conducting box of size  $33 \times 30 \times 6 \text{ mm}^3$  placed on the ground as a battery

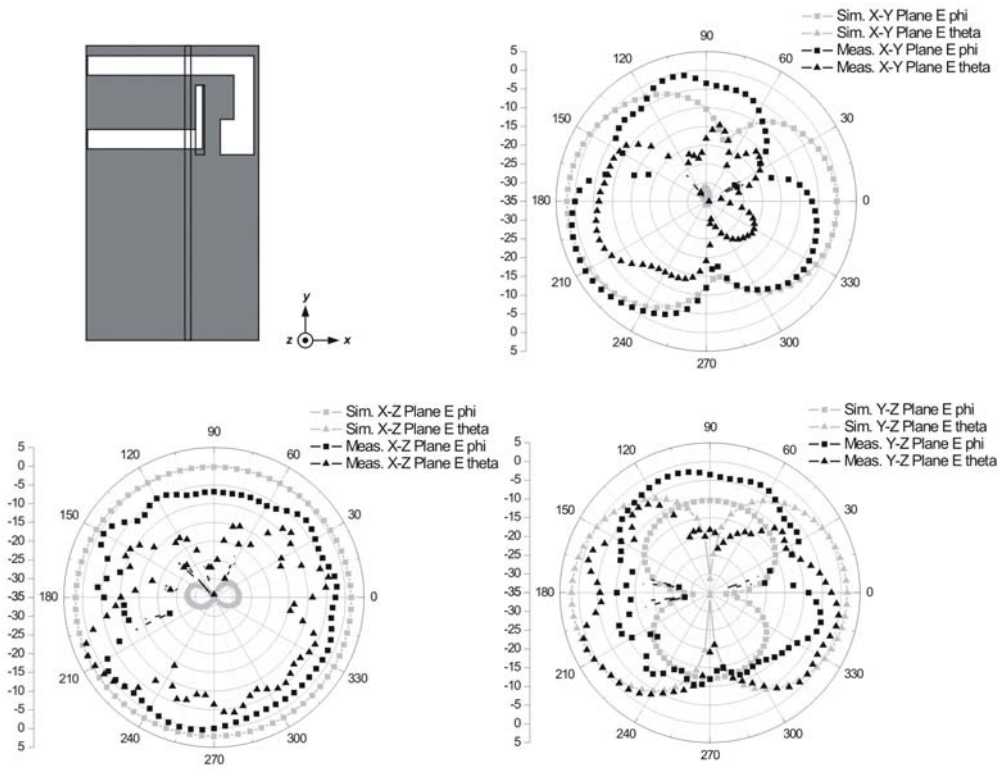
The radiation patterns were measured in a  $7 \times 3.2 \times 3 \text{ m}^3$  anechoic chamber at National Taiwan University of Science and Technology. The measurement was performed by an Agilent E8362B network analyzer along with the NSI 2000 far-field measurement software. Fig. 4.12 illustrates the simulated and measured radiation patterns. The agreement between the simulations and measurements is fairly good in most of the results. The measured peak gains at 900 MHz, 1800 MHz, 2050 MHz, 2450 MHz, 2600 MHz, and 5200 MHz are listed in Table 4.II.

frequency Plane	X-Y	X-Z	Y-Z
900 MHz	0.7	1.0	-0.2
1800 MHz	2.2	2.1	1.2
2050 MHz	1.9	0.1	1.6
2450 MHz	1.6	0.3	-0.4
2600 MHz	1.8	0.4	0
5200 MHz	1.1	-1.0	0.4

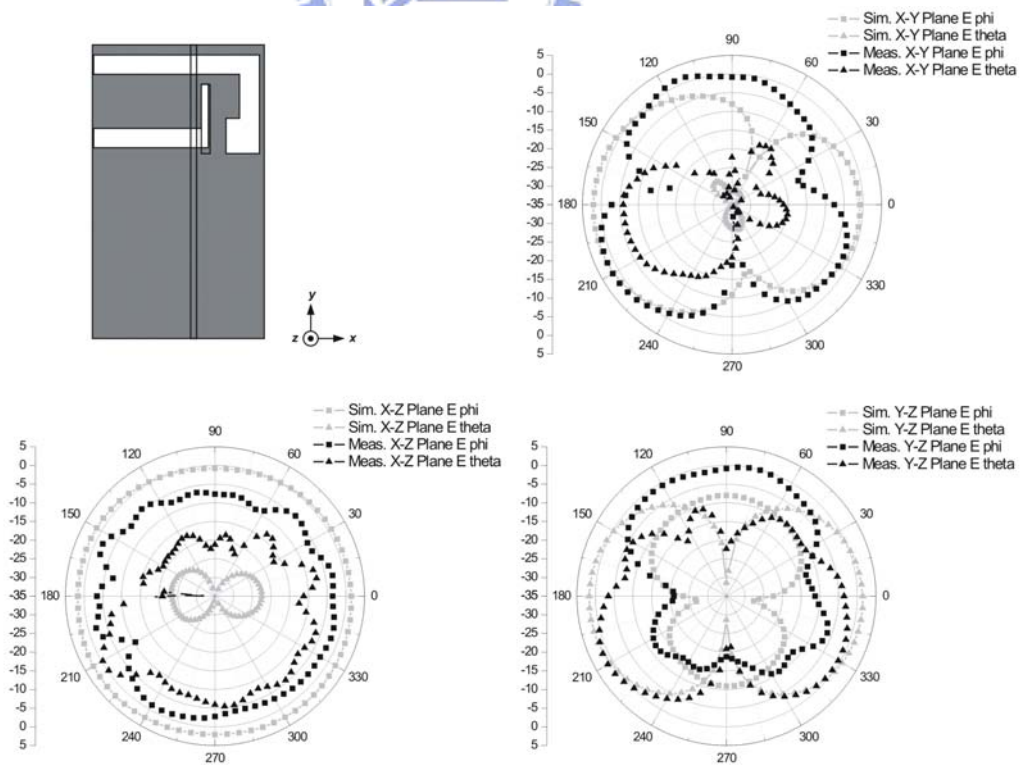
Table 4.II Peak Gain (Unit: dBi)



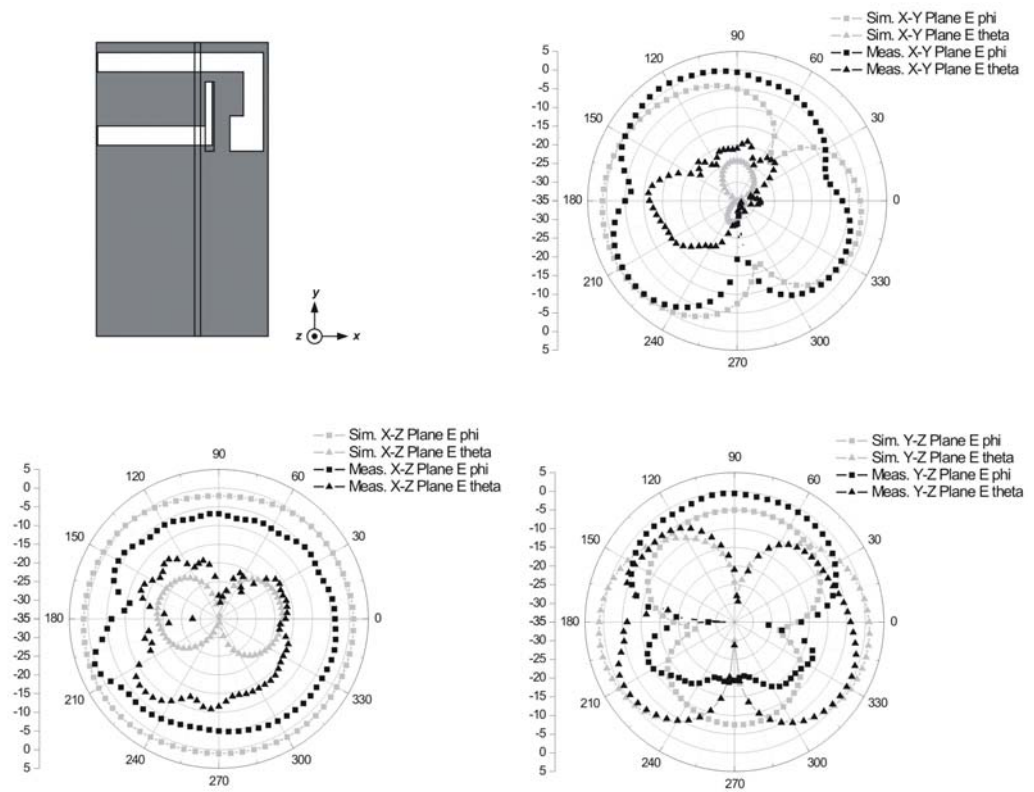
(a) 900 MHz



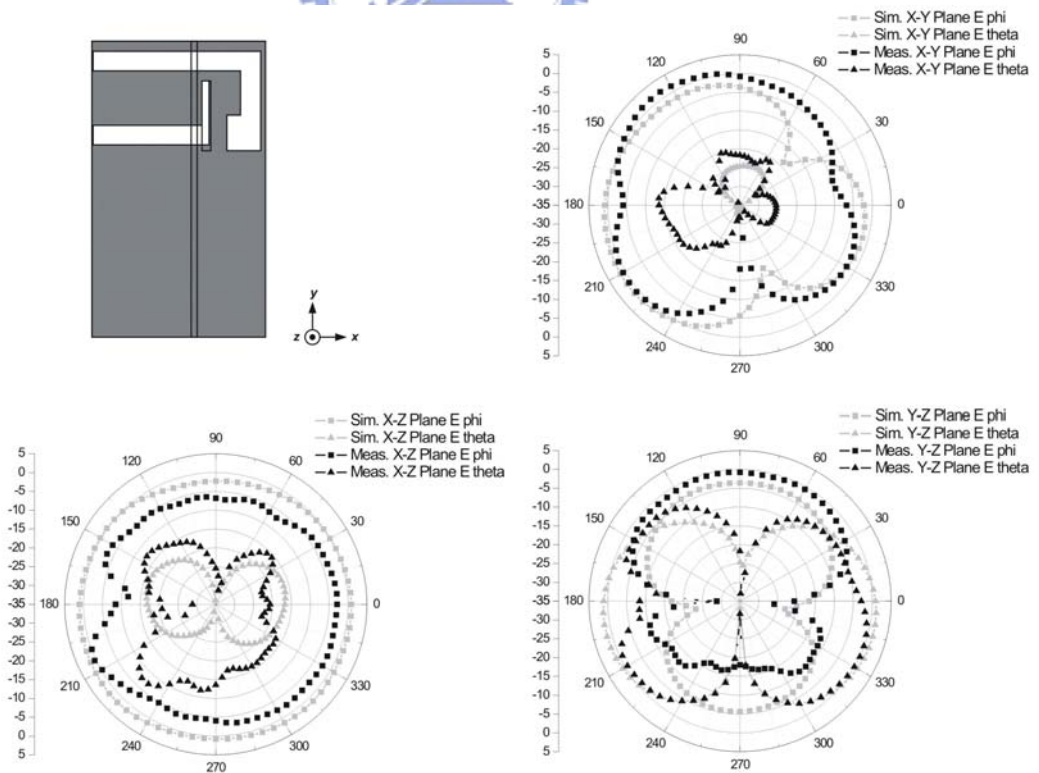
(b) 1800 MHz



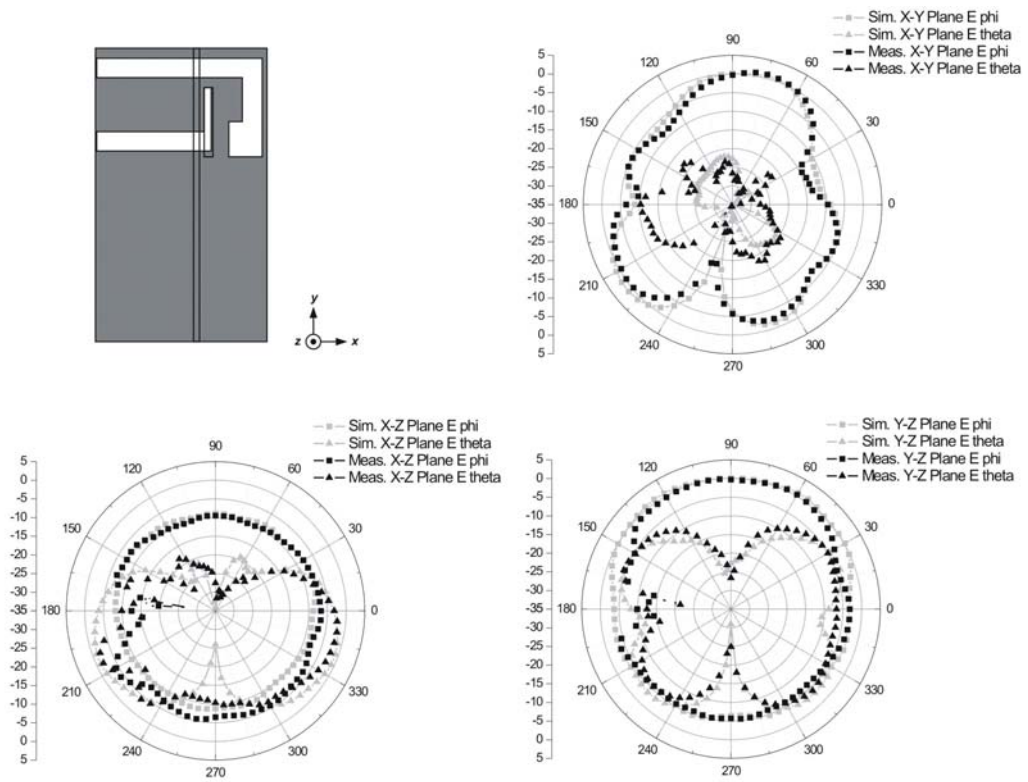
(c) 2050 MHz



(d) 2450 MHz



(e) 2600 MHz



(f) 5200 MHz

Fig. 4.12 Simulated and measured radiation patterns

#### 4.4 Summary

	Antenna size	Ground size	bands
[14] 2008	$36*15.8*6=3413\text{mm}^3$	$65*36=2340\text{mm}^2$	4
[15] 2007	$30*15*4=1800\text{ mm}^3$	$45*100=4500\text{ mm}^2$	7
[16] 2008	$40*5*5=1000\text{ mm}^3$	$40*65=2600\text{ mm}^2$	4
[2] 2007	$40*15*0.8=480\text{ mm}^3$	$40*100=4000\text{ mm}^2$	6
<b>This work 2009</b>	<b><math>35*22*0.8=616\text{ mm}^3</math></b>	<b><math>35*60=2100\text{ mm}^2</math></b>	<b>8</b>

Table 4.III Comparison I

	Innovation
Slot [2] 2007	A microstrip feedline excites the two slots to generate multiband.
<b>Slot (This work)</b>	<ol style="list-style-type: none"> <li><b>1. The broad bandwidth can be achieved by the L-Shaped slot easily.</b></li> <li><b>2. The higher band is generated by the parasitic strip. The parasitic strip avoids the degradation of the mutual coupling between slots and the smaller ground size.</b></li> </ol>

Table 4.IV Comparison II

## Chapter 5 Conclusion

---

A printed slot antenna for internal multiband mobile phone antenna has been proposed and demonstrated. The antenna has a simple structure and is easy to be printed on the top portion of the system circuit board of the mobile phone. In addition, although the antenna shows a simple structure and compact volume, it can generate three bands covering the GSM/DCS/PCS/UMTS/WiMAX/WLAN operation, and good radiation characteristics over the operating bands have been obtained. The present antenna does not contain the effect of the user's head and hand on the antenna impedance and pattern characteristics. The effect of the operator head and hand on the proposed antenna is planned to be discussed in the future. In addition, the proposed antenna is EM compatible with the nearby components. Hence, the proposed printed slot antenna is suitable for application in the modern thin mobile phones as an internal antenna.

---

---

## References

---

- [1] K. L. Wong, *Planar Antennas for Wireless Communications*. New York: Wiley, 2003.
- [2] Chun-I Lin and Kin-Lu Wong, "Printed Monopole Slot Antenna for Internal Multiband Mobile Phone Antenna," *IEEE Trans. Antennas Propag.*, vol. 53, pp. 3690–3697, Dec. 2007.
- [3] Kin-Lu Wong and Li-Chun Lee, "Multiband printed monopole slot antenna for WWAN operation in the laptop computer," *IEEE Trans. Antennas Propag.*, vol. 57, pp. 324–330, Feb. 2009.
- [4] A. Ishimaru, *Electromagnetic wave propagation, radiation, and scattering*, Prentice-Hall, 1991.
- [5] John D. Kraus and Ronald J. Marhefka, *Antenna for all application*, 3rd ed. McGraw-Hill, 2003.
- [6] C. A. Balanis, *Antenna theory*, 3rd ed. Wiley, 2005.
- [7] K. C. Gupta, P. Garg, I. Bahl, and P. Bhartia, *Microstrip lines and slotlines*, 2nd ed. Norwood, MA: Artec House, 1996.
- [8] R. Azadegan and K. Saraband, "A novel approach for miniaturization of slot antennas," *IEEE Trans. Antennas Propag.*, vol. 51, pp. 421–429, Mar. 2003.
- [9] N. Behdad and K. Sarabandi, "A wide-band slot antenna design employing a fictitious short circuit concept," *IEEE Trans. Antennas Propag.*, vol. 53, pp. 475–782, Jan. 2005.
- [10] Saeed I. Latif, Lotfollah Shafai, and Satish Kumar Sharma, "Bandwidth enhancement



- and size reduction of microstrip slot antennas,” *IEEE Trans. Antennas Propag.*, vol. 53, pp. 994-1003, Mar. 2005.
- [11] Wen-Shan Chen and Kuang-Yuan Ku, “Band-rejected design of the printed open slot antenna for WLAN/WiMAX operation,” *IEEE Trans. Antennas Propag.*, vol. 56, pp. 1163-1169, Apr. 2008.
- [12] Hyungrak Kim and Young Joong Yoon, “Microstrip-fed slot antennas with suppressed harmonics,” *IEEE Trans. Antennas Propag.*, vol. 53, pp. 2809-2817, Sep. 2005.
- [13] Jen-Yea Jan and Liang-Chih Tseng, “Small planar monopole antenna with a shorted parasitic inverted-L wire for wireless communications in the 2.4-, 5.2-, and 5.8-GHz bands,” *IEEE Trans. Antennas Propag.*, vol. 52, pp. 1903-1905, Jul. 2004.
- [14] Seokjin Hong, Wonseob Kim, Hoon Park, Sungtek Kahng, and Jaehoon Choi, “Design of an internal multiresonant monopole antenna for GSM900/DCS1800/US-PCS/S-DMB operation,” *IEEE Trans. Antennas Propag.*, vol. 56, pp. 1437-1443, May. 2008.
- [15] Rashid Ahmad Bhatti and Seong Ook Park, “Hepta-band internal antenna for personal communication handsets,” *IEEE Trans. Antennas Propag.*, vol. 55, pp. 3398-3403, Dec. 2007.
- [16] Yun-Wen Chi and Kin-Lu Wong, “Compact multiband folded loop chip antenna for small-Size mobile phone,” *IEEE Trans. Antennas Propag.*, vol. 56, pp. 3797–3803, Dec. 2008.